Received June 30, 2021, accepted July 14, 2021, date of publication July 30, 2021, date of current version August 12, 2021.

Digital Object Identifier 10.1109/ACCESS.2021.3101419

Multiperiod Optimum Power Flow for Active Distribution Networks With Provisioning of Ancillary Services

THAÍS M. BLASI[1], THELMA S. P. FERNANDES[1], ALEXANDRE R. AOKI[1], (Senior Member, IEEE), AND FABRÍCIO H. TABARRO[2]

[1]Department of Electrical Engineering, Federal University of Paraná, Curitiba, Paraná 82590-300, Brazil
[2]Department of Service Channels Technology and Quality, Companhia Paranaense de Energia—COPEL Distribution, Curitiba, Paraná 81200-240, Brazil

Corresponding author: Thaís M. Blasi (thaisblasi95@gmail.com)

This work was founded by Compania Paranaense de Energia—COPEL Research and Technological Development (RTD) Program regulated by the Brazilian Electricity Regulatory Agency (ANEEL) under Project PD-02866-0511/2019, being supported in part by the Technology Development of CNPQ—National Council for Scientific and Technological Development through the Ministry of Science, Technology, Innovations, and Communications, and in part by the CAPES—Brazilian Federal Agency for Support and Evaluation of Graduate Education through the Ministry of Education of Brazil.

ABSTRACT Distribution networks are suffering a transformation process with the insertion of distributed energy resources, changing from a passive part of the power grid into an active system. Aiming to reduce the challenges for the distribution system operators to keep the power grid operating inside of the quality levels it is possible to propose some ancillary services. Optimum Power flow is an optimization method used to plan the distribution grid operation. Additionally, the distributed energy resources can be modeled on it and ancillary services provisioning can be considered, as proposed in this work. In this way, the objective of the present work is to formulate a Multiperiod Optimum Power Flow (MPOPF) with the insertion of distributed generation, energy storage systems, microgrids, and electric vehicles at the distribution grid. This MPOPF considers the provisioning of ancillary services by the inverters associated with the equipment connected to the main grid. In the formulation, the entire grid is modeled, considering the placement of classic equipment as a voltage regulator and capacitor banks, in addition to modern technologies as DFACTS (Distribution - Flexible AC Transmission System) and four-quadrant inverters. The MPOPF was simulated for several scenarios considering a 90-bus test feeder and a real distribution grid from Curitiba – Brazil. From the results, the MPOPF proved to be highly robust, being able to simulate the grid with all the equipment connected simultaneously, performing the optimal dispatch of active and reactive power, as well as allowing the operation of ancillary services such as voltage support, peak-shaving, and demand-side management.

INDEX TERMS Active distribution network, ancillary service, DFACTS, distributed energy resource, multiperiod optimum power flow.

I. INTRODUCTION

Significantly changes have been happening in distribution systems, being driven by the power system transformation based on 3Ds trends: decarbonization, decentralization, and digitalization. Those three points are being achieved mostly due to the growth of Distributed Energy Resources (DER), such as distributed generation, energy storage systems, electric vehicles, flexible loads, and microgrids, implemented at the distribution network level. These resources bring more flexibility, security, efficiency, and challenges for the power grid operation, regarding power quality levels.

The associate editor coordinating the review of this manuscript and approving it for publication was Payman Dehghanian.

The challenges faced by the power utilities are attributable to the DERs that bring many changes, as the two-way power flow, new technical configurations, new business models, and the growth of grid digitalization [1]. This new power grid is named Active Distribution Network (ADN) since it is not anymore just a passive system, responsible only for deliver power, but it is a system able to be active in providing power, managing, and controlling power flow [2].

Thus, power utilities are looking for new planning, operation, and control systems that can integrate the DERs with the least impact, and when possible, contribute to improving power grid operation.

Different techniques can be used to proposed optimizations to power system, being one of them the Optimum Power

This work is licensed under a Creative Commons Attribution 4.0 License. For more information, see https://creativecommons.org/licenses/by/4.0/

Flow (OPF), which determines the optimum operating state of the power grid based on an optimization problem defined by an objective function, that represents the main goal of the optimization, such as minimize costs, losses, load shedding, voltage deviations, etc.; and constraints, defined by equalities and/or inequalities, representing operational limits and power balance [3]. When multiple numbers of periods with dependency between them are be simultaneously analyzed inside a time horizon, a multiperiod approach of the OPF can be used.

As an optimization problem, the OPF can be solved by different strategies, from conventional methods, like linear and nonlinear programming, quadratic programming, Newton's method, and interior points, or even be done using artificial intelligence techniques as particle swarm, human or physics-inspired techniques, evolutionary optimization or neural networks [4].

Ongoing to improve DERs integration on the distribution grid, new OPF approaches have been proposed, considering different targets to be optimized and different scenarios to be analyzed.

Aiming to improve active and reactive power dispatch, the work proposes by [5] has separated the optimization problem into two sub-problems: one for active and another for reactive power. Using this approach, the authors proposed an optimum power flow to minimize power losses and improve voltage levels, considering a battery energy storage operation.

The work developed by [6] proposes a multi-period optimum power flow to reduce the energy costs and the aging of a battery energy storage system (BESS) considering three different time horizons: a forecast stage, a predictive optimization stage, and a local control stage.

Works developed by [7]–[11] consider the development of optimum power flow for grid optimization with the insertion of distributed energy resources, as distributed generation, in addition to optimize the dispatch of BESS placed on the system. In [7] the optimization is solved by extended semi-defined program relaxations, being an equivalent process to Lagrangean dual. Reference [8] solves a multi-period OPF using the GAMS software (optimization solver programming language using algebraic notation). Reference [9] represents the battery and power grid constraints along the simulation periods using a Fourier coefficient vector, being aggregated to the rest of the nonlinear optimization problem solved using the interior points method. The work proposed by [10] considers multiple generators and batteries on the distribution grid solving the optimization problem using an expanded Lagrangean approach with KKT (Karush-Kuhn-Tucker optimization base conditions). At least, [11] solves the optimization problem of its OPF using dynamic programming techniques, resulting in the optimum scenario of grid and battery dispatch.

The work developed by [12] proposes a multiperiod AC Optimum Power Flow for a smart grid with DERs considering the provisioning of ancillary services, regarding grid voltages and congestions issues. To solve the optimum power flow it was used a mixed-integer nonlinear model (MINLP) via Julia programming language. It was added the stochasticity of the wind/solar generation using an auto-regressive integrated moving average. In this paper the authors modeled a 34-bus test feeder, including the optimization of the on-line tap change (OLTC) transformer at the substation bus, two flexible loads, three energy storage systems and eight distributed generation with solar and wind. For the objective function authors aimed to minimize the costs related to active power curtailed of distributed generation (DG), energy storage usage, power demand flexibility and costs of OLTC operation. In this case the reactive dispatch is proposed only for the DG units using a power factor control strategy. From the results, it was verified that the location of the energy storage, in addition to the operation of the DGs, can contribute to minimize the load curtailment under different conditions.

In [13], the authors considered the real case of a smart grid in the European inteGRIDy project, which is modeled as a microgrid for the study that aims to evaluate the impacts of DGs and the benefits from energy storage systems (ESS). The approach of the article is to develop an OPF to control the ESS itself and after integrated to an OLTC, considering a distribution grid with distributed generation systems and demand-side management. In this case, it is aimed to minimize the operational costs from generators and from ESS, as well as maximize the DG contribution. For the OPF it is considered the power constraints related to active and reactive power dispatch, being controllable by the apparent power limits. Considering different configurations, it is seen voltage levels improvement and reduction of tap changes as much reactive dispatch is considered. Additionally, the ESS contributes to the power flow management, allowing the maximization of DG power provisioning.

Besides the provisioning of ancillary services is the reactive power dispatch, that could be performed by equipment with inverters and conventional equipment as capacitor banks. However, there is another possibility that can dispatch reactive power into the grid, that is the power electronic devices named FACTS (Flexible AC Transmission Systems).

On the OPF approach, some works included the usage of FACTS, however, most of them consider the transmission systems, as done in [14], [15]. Recently, various manufacturers started to developed FACTS applicable to distribution systems, named D-FACTS (Distribution - Flexible AC Transmission System) since more and more the voltage control is becoming a challenge due to the transformations that are happening in this grid level. The work developed by [16] proposes an optimum power flow with the allocation of Series Static Voltage Restores (SSVR) in distribution grids with photovoltaic systems (PV). The SSVR is modeled to allow the adjustment of line series reactance or inject/absorb power from the distribution grid, contributing to voltage levels improvement. The OPF proposed in [14] was solved using IPOPT (Interior Point Optimizer) open-source software.

Regarding the usage of D-FACTS in Active Distribution Networks, [17] presents the main advantages of D-FACTS

usage at distribution networks, focusing on the D-SVC (Distributed Static Var Compensator). This equipment is based on conventional thyristors, able to generate or absorb reactive power by the exchange of capacitive or inductive current. This behavior can be modeled as an adjustable reactance for steady-state analysis, being controllable according to power grid needs. The authors propose the entire formulation for D-SVC modeling at distribution system power flow, being implemented at Matlab and tested for a 69-bus distribution feeder. From the results, it is noticed the effectiveness of the D-SVC usage for voltage control, even when DG is considered.

In a way to contribute to the planning of voltage regulation via reactive power dispatch of ADNs, the present work proposes a Multiperiod Optimum Power Flow (MPOPF) to optimize the day-ahead planning of an ADN, which presents distributed generation, energy storage, flexible loads, and microgrids. These elements are modeled to allow the optimization of their active and/or reactive power dispatch. Additionally, the distribution grid is completely modeled, considering voltage regulators, capacitor banks, and D-FACTS, which operations are also optimized by the MPOPF proposed.

The nonlinear optimization problem is modeled by the definition of a multi-objective function, that aims to minimize power losses, costs and simultaneously maximize load supply for flexible loads and microgrids. In addition, operational constraints are defined by equalities and inequalities expressions representing the operative limits of the grid and the considered equipment. The MPOPF is solved by the Interior-Points Method [18]–[21] in a Primal-Dual version completely implemented in Python language, without use any solver.

The main contributions of this paper are:

- technical analysis of an active distribution network, with multiple elements being considered simultaneously;
- evaluation of power grid operation with different scenarios and elements being considered, as well as the possibility of the ancillary services provisioning;
- the proposition of a OPF model that realizes the reactive power dispatch from DERs, i.e., from PVs and BESS, using the apparent power limits;
- the introduction of the D-SVC operation and optimization on the OPF formulation;
- implementation into two different power systems, being a test feeder and a real distribution grid representing the possibility of MPOPF applications in systems with a high number of buses;

strategies implementation to improve computational time, mainly when a real distribution grid is modeled.

For the simulations, initially, a 90-bus distribution test feeder is considered, with different scenarios of DERs placement and ancillary services provisioning. From all scenarios, the results of power losses, voltage levels, reverse power flow, and operational costs are analyzed being compared at the end to each other and the base case, corresponding this one to the conventional distribution network, with no DERs.

At least, a real distribution feeder from Curitiba (Brazil) with 314 buses is simulated considering some of the scenarios proposed initially for the test feeder, allowing to analyze how does a real system would operate when it became an ADN.

In this way it is possible to evaluate the behavior of the proposed methodology when it considers a grid with greater complexity and/or dimension.

This paper is organized as follows: Section 2 presents the elements of an AND, concepts, and examples of ancillary services. Section 3 describes the MPOPF formulation, with the definition of the input and control variables, the objective function, and the operational constraints. Section 4 presents system characteristics for the simulated circuits, both test feeder and real distribution grid, as well the description of the equipment that will be evaluated. Section 5 presents the 90 buses test feeder simulation results, followed by Section 6 with the MPOPF results for the real circuit. Finally, Section 7 describes the conclusions.

II. ACTIVE DISTRIBUTION NETWORKS AND ANCILLARY SERVICES

There are many definitions of active distribution networks, however in general it means power grids that can control and coordinate their operation in addition to Distributed Energy Resources.

In the context of distributed generation systems, one of the most considered is photovoltaic generation. In Brazil, for example, at the beginning of May 2021, there was more than 472,468 PV distributed generation systems, totalizing more than 5,509 MW of installed power [22].

With the connection of these systems, new market strategies needed to be adopted, to price the injection of active power into the grid, stimulating system owners to inject as much active power as possible. Nevertheless, as the number of distributed generation systems increase, more problems start to happen on the power grid, and more difficult to keep the system operating inside of power quality levels.

Aiming to improve distribution grid operation, ancillary services are becoming more necessary, and they could be provided in different ways and by different actors.

Ancillary service was a concept applied only at transmission levels, but with the transformation of the distribution grids, it started to be requested in this part of the power grids also [23].

Among ancillary services, there are voltage support, demand response, emergency frequency response, grid resiliency and flexibility, and many others.

Regarding voltage support, one of the strategies is reactive power control, which can be performed by equipment with four-quadrant inverters, or even power electronic devices as D-FACTS.

In the case of PVs with four-quadrant inverters, there is the possibility to operate providing/absorbing reactive power independently of the solar generation. However, it is

important to highlight that nowadays, most parts of electricity markets do not remunerate this reactive injection, being not attractive to the system owner.

Battery systems are also connected to distribution grids by inverters, that could operate in four-quadrant mode, and can realize some ancillary services to the power grid also. In this case, as the system can control the active and reactive power injection/absorb, it is possible to realize the voltage support (by active and reactive power control), load-leveling (relieving peak load periods of the feeder and increasing load in periods of lower demand), and load peak shaving (reducing the peak demand of distribution feeder). Since BESS can be owned by power utilities, its operation can be defined to supply the biggest issues of the power grid.

The use of FACTS in distribution grids is brand new and is becoming more attractive as grids become more complex and have more DERs connected. According to some manufacturers, the main benefits of D-FACTS usage consist of fast voltage regulation, damping of active power oscillations, and increase of power flow through AC lines.

There are many equipment technologies, however for the present work a D-SVC was chosen, due to the compatibility of voltage level, sizing, and because of the possibility to inject or absorb reactive power from the grid, controlling bus voltage, and providing voltage support. According to [24] several studies have been carried out considering the insertion of D-SVCs in feeders that present distributed generation. In addition, some articles reviewed in [24] show that the allocation of D-SVCs contributed to the improvement of voltage levels and reduction of power losses.

Another ancillary service is the Demand Side Management (DSM), which consists of the managing of flexible loads, according to grid necessities, cutting these loads suppling in some periods, or shifting this demand for periods, in which the system has a low load. This kind of ancillary service requires specific load contracts as well the communication between load and Distribution System Operator (DSO).

When microgrids are connected to the grid, they operate as a flexible load, however with the possibility to provide power to the main system. In this way, it is possible to perform a DSM with microgrids proposed behavior, which arise from the internal optimization and control, and that should be informed to the DSO. With this information, DSO can evaluate the entire grid operation and, if some power quality problems are faced, a DSM can propose a new scheduled behavior for the microgrid, that will re-optimize its operation, considering the DSO recommendations.

The microgrid behavior can also provide some ancillary services to the power grid, as voltage support, peak shaving, and load leveling, depending on its periods operating as loads or generators.

It is important to emphasize that for ancillary systems be viable in distribution networks it is essential to have equipment with technology and control that allow this type of operation aligned with power utilities. In addition, regulation and market must be updated for this type of service.

In the next section, all elements described as ancillary service providers will be modeled on a Multiperiod Optimum Power Flow, used to plan a day ahead operation of a distribution feeder.

III. MULTIPERIOD OPTIMUM POWER FLOW

The classical objective of an OPF is determines an optimal operational point for a given instant of time, aiming to establish, among other interests, the power injection in all system buses. Generally, the OPF objective function corresponds to the optimization of power grid operation in a specific condition, whereas the multiperiod approach realizes the optimization considering, simultaneously, several periods.

The formulation proposed for the present work was based on [21] that minimizes the system power losses and costs in a hydrothermal pre-dispatch problem, implementing an MPOPF solved using Interior Points Method with a Primal-Dual Version. Works developed by [25] follow the same approach considering it for a distribution system with the insertion of distributed energy resources as distributed generation, batteries, and electric vehicles.

MPOPF formulation is based on input and control variables. The definition of the objective function, and the power systems operation constraints are presented in the sequence.

A. INPUT VARIABLES

Input variables are the ones related to system structure, being expressed for each bus, line, or equipment, being previously defined and responsible for the characterization of the scenario in which the optimization will be performed.

For the active and reactive power demand in all buses (number of buses - *nb*), vectors **Pd** and **Qd** are respectively defined for each of the total numbers of periods (*nper*) considered. These vectors have information of fixed and manageable demand powers and their sizing corresponds to (*nb.nper* x 1).

$$\mathbf{Pd} = \begin{bmatrix} Pd_1^1 \\ \vdots \\ Pd_{nb}^1 \\ \vdots \\ \vdots \\ Pd_1^{nper} \\ \vdots \\ Pd_{nb}^{nper} \end{bmatrix} \quad \mathbf{Qd} = \begin{bmatrix} Qd_1^1 \\ \vdots \\ Qd_{nb}^1 \\ \vdots \\ \vdots \\ Qd_1^{nper} \\ \vdots \\ Qd_{nb}^{nper} \end{bmatrix} \tag{1}$$

where:

Pd_i^k: represents the inflexible active power demanded at bus i and period k;

Qd_i^k: represents the inflexible reactive power demanded at bus i and period k.

The inflexible demand value of each bus and period of the day (24 hours) depicts the behavior of the loads along with the analysis.

Microgrids, that corresponds to part of the grid that present generation and storage systems and can operate disconnected

from the main grid, are seen as a flexible load, from the grid MPOPF point of view. In this case, another load profile is considered at this point of connection, presenting positive values, when its behavior is of load, denying energy from the grid, negative values when it injects power in the grid, operating as a generation, and null values when considered islanded operation, being disconnected from the main grid.

The definition of the flexible loads is given in another vector, ***FPd***,that presents the list of foreseen flexible buses that have the possibility of demand managing:

$$\boldsymbol{FPd} = \begin{bmatrix} FPd_1^1 \\ \vdots \\ FPd_{nb}^1 \\ \vdots \\ \vdots \\ FPd_1^{nper} \\ \vdots \\ FPd_{nb}^{nper} \end{bmatrix} \boldsymbol{FQd} = \begin{bmatrix} FQd_1^1 \\ \vdots \\ FQd_{nb}^1 \\ \vdots \\ \vdots \\ FQd_1^{nper} \\ \vdots \\ FQd_{nb}^{nper} \end{bmatrix} \tag{2}$$

where:

FPd_i^k: ideal flexible active power demanded at bus i and period k;

FQd_i^k: ideal flexible reactive power demanded at bus i and period k.

Regarding electric mobility, the applications such as V2G (vehicle-to-grid) are not being considered and the electric vehicle charging stations in the grid are portrayed as load. In this case, the difference is due to the behavior of the load curve used, aiming to represent the power demanded to charge the vehicle at each instant of time.

Regarding the integration of photovoltaic systems (PV) as distributed generation, its active power output is considered an input variable for the MPOFP. Since it major depends on solar irradiation and considering a day-ahead scenario, its behavior can be estimated based on the weather forecast. Nowadays, the techniques used for weather estimation are very trustworthy, resenting a reliability of 98% [26]. With the irradiation forecasted information and knowing the installed power of the PV systems located along the feeder it is possible to calculate the solar active power (***Pgsun***) provisioning in each bus for all the analysis periods:

$$\boldsymbol{Pgsun} = \begin{bmatrix} Pgsun_1^1 \\ \vdots \\ Pgsun_{nb}^1 \\ \vdots \\ \vdots \\ Pgsun_1^{nper} \\ \vdots \\ Pgsun_{nb}^{nper} \end{bmatrix} \tag{3}$$

where:

$Pgsun_i^k$: active photovoltaic power injected at bus i and period k.

The PV system reactive power (***Qgsun***) can be calculated by the power factor (pf) considered for the power system inverter responsible for the connection of the generation system to the grid. In most cases of real applications, the power factor is one, which corresponds to the injection of only active power. However, the reactive power injection can be useful to improve power grid operation, as providing voltage support. In this case, the solar reactive power will be an optimized variable that depends on the limits of the apparent power of the inverters (**Ssun**):

$$\mathbf{Ssun} = \begin{bmatrix} Ssun_1^1 \\ \vdots \\ Ssun_{nb}^1 \\ \vdots \\ \vdots \\ Ssun_1^{nper} \\ \vdots \\ Ssun_{nb}^{nper} \end{bmatrix} \tag{4}$$

where:

$Ssun_i^k$: apparent photovoltaic power injected at bus i and period k.

Other input variables are generation units active (***Pg$_{max}$*** and ***Pg$_{min}$***) and reactive (***Qg$_{max}$*** and ***Qg$_{min}$***) power limits, excluding distributed generation in this case. The power provisioning limits from the substation are included in those vectors, since it actuates as a power source for the distribution system, corresponding to a generation system connected to bus 1:

$$\boldsymbol{Pg_{max}} = \begin{bmatrix} {Pg_{max_1}}^1 \\ \vdots \\ 0 \\ \vdots \\ \vdots \\ {Pg_{max_1}}^{nper} \\ \vdots \\ 0 \end{bmatrix} \boldsymbol{Qg_{max}} = \begin{bmatrix} {Qg_{max_1}}^1 \\ \vdots \\ 0 \\ \vdots \\ \vdots \\ {Qg_{max_1}}^{nper} \\ \vdots \\ 0 \end{bmatrix} \tag{5}$$

where:

${Pg_{max_1}}^k$ and ${Qg_{max_1}}^k$: maximum limits of the active and reactive power injected by the substation at bus 1 and period k, respectively.

Voltage magnitude limits (***V$_{max}$*** and ***V$_{min}$***) should also be provided for all buses in all periods. It is important to highlight that the voltage limits will not necessarily be the same over the whole period and nor will it be the same for all buses in the circuit, as it may depend, for example, on the

grid load levels:

$$\boldsymbol{V_{max}} = \begin{bmatrix} vmax_1^1 \\ \vdots \\ vmax_{nb}^1 \\ \vdots \\ \vdots \\ vmax_1^{nper} \\ \vdots \\ vmax_{nb}^{nper} \end{bmatrix} \boldsymbol{V_{min}} = \begin{bmatrix} vmin_1^1 \\ \vdots \\ vmin_{nb}^1 \\ \vdots \\ \vdots \\ vmin_1^{nper} \\ \vdots \\ vmin_{nb}^{nper} \end{bmatrix} \tag{6}$$

where:

$v_{max_i}^k$ and $v_{min_i}^k$: maximum and minimum limits of the voltage magnitude at bus i and period k; respectively.

Correlated with voltage boundary, there are the limits of voltage regulator taps ($\boldsymbol{a_{max}}$ and $\boldsymbol{a_{min}}$). The voltage regulators are allocated in series with a line:

$$\boldsymbol{a_{max}} = \begin{bmatrix} {a_{max_1}}^1 \\ \vdots \\ {a_{max_{nl}}}^1 \\ \vdots \\ \vdots \\ {a_{max_1}}^{nper} \\ \vdots \\ {a_{max_{nl}}}^{nper} \end{bmatrix} \boldsymbol{a_{min}} = \begin{bmatrix} {a_{min_1}}^1 \\ \vdots \\ {a_{min_{nl}}}^1 \\ \vdots \\ \vdots \\ {a_{min_1}}^{nper} \\ \vdots \\ {a_{min_{nl}}}^{nper} \end{bmatrix} \tag{7}$$

where:

${a_{max_j}}^k$ and ${a_{min_j}}^k$: maximum and minimum limit of the voltage regulator taps of line j and period k, respectively;

nl: number of lines.

Moreover, there is the information regarding the susceptance capacitance of capacitor banks ($\boldsymbol{Bsh}$):

$$\boldsymbol{Bsh} = \begin{bmatrix} Bsh_1^1 \\ \vdots \\ Bsh_{nb}^1 \\ \vdots \\ \vdots \\ Bsh_1^{nper} \\ \vdots \\ Bsh_{nb}^{nper} \end{bmatrix} \tag{8}$$

where:

Bsh_i^k: the susceptance capacitive of capacitor banks at bus i and period k.

The $\boldsymbol{Bsh}$ vector corresponds to the static capacitor banks that are considered connected or disconnected from the main grid, without control during the optimization performance.

However, it is possible to optimize the input or output of reactive power dispatch using D-FACTS. These systems can contribute to control voltage levels, as well as improve system reliability [27], [28]. So, it is necessary to define the maximum value of susceptance capacitive (which will be represent the injected reactive power to the grid), $\boldsymbol{Bst_{max}}$, and the minimum value of susceptance capacitive (which will be represent the absorbed reactive power from the grid), $\boldsymbol{Bst_{min}}$. These values are defined according to the sizing of the considerable D-SVC:

$$\boldsymbol{B_{st_{max}}} = \begin{bmatrix} {B_{st_{max_1}}}^1 \\ \vdots \\ {B_{st_{max_{nl}}}}^1 \\ \vdots \\ \vdots \\ {B_{st_{max_1}}}^{nper} \\ \vdots \\ {B_{st_{max_{nl}}}}^{nper} \end{bmatrix} \boldsymbol{B_{st_{min}}} = \begin{bmatrix} {B_{st_{min_1}}}^1 \\ \vdots \\ {B_{st_{min_{nl}}}}^1 \\ \vdots \\ \vdots \\ {B_{st_{min_1}}}^{nper} \\ \vdots \\ {B_{st_{min_{nl}}}}^{nper} \end{bmatrix} \tag{9}$$

where:

Bst_i^k: represents the maximum limit of susceptance capacitive of D-SVC at bus i and period k.

As a D-SVC is a shunt element, it was modeled in a similar way to the capacitor banks, however, its reactive power injection is dispatchable according to the grid needs [17].

Finally, the circulating active power flow limits through the lines are given by $\mathbf{F_{max}}$. The minimum active power flow limit is considered as the negative of the maximum active power flow limit:

$$\mathbf{F_{max}} = \begin{bmatrix} Fmax_1^1 \\ \vdots \\ Fmax_{nl}^1 \\ \vdots \\ Fmax_1^{nper} \\ \vdots \\ Fmax_{nl}^{nper} \end{bmatrix} \tag{10}$$

where:

$F_{max_j}^k$: maximum limit of active power flow through the j and period k.

Considering the integration of energy storage systems into distribution grids, more specifically battery energy storage systems (BESS), its behavior and characteristics were also modeled to be part of the MFOPF formulation. Thus, the active power boundaries ($\boldsymbol{P_{bat_{max}}}$ and $\boldsymbol{P_{bat_{min}}}$) should also be defined, regarding the capacity of the storage system to absorb and provide power. Those limits are associated not only with the battery itself but with the power system inverter used to couple the BESS to the main grid. In this way, the reactive power can be defined by the operational power factor considered, as done for PV system, or even can be considered dispatched for the provisioning of

the ancillary services:

$$\boldsymbol{P_{bat_{max}}} = \begin{bmatrix} P_{bat_{max_1}}{}^{1} \\ \vdots \\ P_{bat_{max_{nl}}}{}^{1} \\ \vdots \\ \vdots \\ P_{bat_{max_1}}{}^{nper} \\ \vdots \\ P_{bat_{max_{nl}}}{}^{nper} \end{bmatrix} \boldsymbol{P_{bat_{min}}} = \begin{bmatrix} P_{bat_{min_1}}{}^{1} \\ \vdots \\ P_{bat_{min_{nb}}}{}^{1} \\ \vdots \\ \vdots \\ P_{bat_{min_1}}{}^{nper} \\ \vdots \\ P_{bat_{min_{nb}}}{}^{nper} \end{bmatrix} \quad (11)$$

where:

$Pbat_{max_i}{}^{nper}$ and $Pbat_{min_i}{}^{nper}$: maximum and minimum limits of the active power of BESS at bus i and period k; respectively. It can be used $\boldsymbol{P_{bat_{min}}} = -\boldsymbol{P_{bat_{max}}}$.

Energy stored capacity should also be defined ($\boldsymbol{EBAT_{max}}$ and $\boldsymbol{EBAT_{min}}$) being the upper boundary related to system sizing (kWh) and the lower boundary dependent on the depth-of-discharge (DoD) defined by the system owner:

$$\boldsymbol{EBAT_{min}} = \begin{bmatrix} Ebat_{min_1}{}^{1} \\ \vdots \\ Ebat_{min_{nb}}{}^{1} \\ \vdots \\ \vdots \\ Ebat_{min_1}{}^{nper} \\ \vdots \\ Ebat_{min_{nb}}{}^{nper} \end{bmatrix}$$

$$\boldsymbol{EBAT_{max}} = \begin{bmatrix} Ebat_{max_1}{}^{1} \\ \vdots \\ Ebat_{max_{nb}}{}^{1} \\ \vdots \\ \vdots \\ Ebat_{max_1}{}^{nper} \\ \vdots \\ Ebat_{max_{nb}}{}^{nper} \end{bmatrix} \quad (12)$$

where:

$Ebat_{max_i}{}^{k}$ and $Ebat_{min_i}{}^{k}$: maximum and minimum limits of energy stored capacity of BESS at bus i and period k; respectively. It can be established in $EBAT_{min_i}{}^{nper}$, the desired values that the BESS must be loaded at the final of the day.

In the same way as PV reactive power, the reactive power of BESS can be useful to improve power grid operation, providing voltage support. In this case, the BESS reactive power will be an optimized variable that depends on the apparent power limits of its inverter:

$$\boldsymbol{Sbat} = \begin{bmatrix} Sbat_1^1 \\ \vdots \\ Sbat_{nb}^1 \\ \vdots \\ \vdots \\ Sbat_1^{nper} \\ \vdots \\ Sbat_{nb}^{nper} \end{bmatrix} \quad (13)$$

where:

$Sbat_i^k$: BESS apparent power injected at bus i and period k.

Besides the aforementioned variables, other information can be defined as input variables, such as: power system parameters; system configurations; reference bus (swing bus); equipment locations; the energy stored in BESS at the start of dispatch period (*Earrive*), and BESS efficiency; tariff values, among others.

The vectors represented in equations (1)-(6), (8), and (11)-(13) have dimensions (*nb.nper* x 1) where *nb* is the number of buses in the grid and *nper* is the number of analyzed periods. Moreover, the vectors presented in equations (7), (9), and (10) have dimensions (*nl.nper* x 1) where *nl* is the number of lines in the grid.

B. CONTROL AND DEPENDENT VARIABLES

All voltage phasors are represented by the rectangular coordinates, as used in [29]:

$$\dot{\boldsymbol{V}} = \begin{bmatrix} \dot{V}_1^1 \\ \vdots \\ \dot{V}_{nb}^1 \\ \vdots \\ \vdots \\ \dot{V}_1^{nper} \\ \vdots \\ \dot{V}_{nb}^{nper} \end{bmatrix} = \begin{bmatrix} e_1^1 \\ \vdots \\ e_{nb}^1 \\ \vdots \\ \vdots \\ e_1^{nper} \\ \vdots \\ e_{nb}^{nper} \end{bmatrix} + j \begin{bmatrix} f_1^1 \\ \vdots \\ f_{nb}^1 \\ \vdots \\ \vdots \\ f_1^{nper} \\ \vdots \\ f_{nb}^{nper} \end{bmatrix} \therefore \dot{\boldsymbol{V}} = e + jf \quad (14)$$

where:

$\dot{V}_i^k$: voltage phasors at bus i and period k;

e_i^k: real component of the voltage $\dot{V}_i^k$;

f_i^k: imaginary component of the voltage $\dot{V}_i^k$.

The elements that compose the real and imaginary components of the bus voltages are grouped as $\boldsymbol{e} = \begin{bmatrix} e_1^1 & \cdots & e_{nb}^{nper} \end{bmatrix}^T$ and $f = \begin{bmatrix} f_1^1 & \cdots & f_{nb}^{nper} \end{bmatrix}^T$ [30].

The vector $\mathbf{x}$ is composed by voltage components of all periods:

$$\mathbf{x} = [\, \mathbf{e} \quad \boldsymbol{f} \,]^{\boldsymbol{T}} \quad (15)$$

where:

$\mathbf{x}$: corresponds to the vector that stores the real and imaginary components of all the bus voltages with dimension (2.*nb.nper* x 1);

T: represents that the vector is transposed.

The rectangular representation is used to overcome the problems of poor numerical conditioning of distribution networks due to short stretches interspersed with excessively long and predominantly radial stretches. Besides that, this rectangular representation results in quadratic active and reactive power balance equations, which facilitate the convergence of the optimization problem [18].

Voltage regulators tap positioning is a controllable variable, since it is defined during the optimization process, as [36]:

$$\mathbf{a} = [\, a_1^1 \;\; \ldots \;\; a_{nb}^1 \;\; \ldots \;\; a_1^{nper} \;\; \ldots \;\; a_{nb}^{nper} \,]^{\boldsymbol{T}} \tag{16}$$

where:

a_j^k: taps position of voltage regulator at line j and period k.

Likewise, the BESS active power behavior is optimized by the MFOPF, which decides the charging ($P_{bat} > 0$) and discharging ($P_{bat} < 0$) periods:

$$\boldsymbol{Pbat} = [\, Pbat_1^1 \cdots Pbat_{nb}^1 \cdots Pbat_1^{per} \cdots Pbat_{nb}^{nper} \,]^{\boldsymbol{T}} \tag{17}$$

where:

$Pbat_i^k$: power active of BESS injected at bus i and period k.

In this work, it is assumed that ideal or predicted values of flexible loads are previously stipulated by their owners (***FPd*** and ***FQd***). If this predicted or ideal flexible load cannot be dispatched, due to technical reasons of the grid, it must be cut off. This is done by the optimization variable, ***gamma,*** that weighs the values of ***FPd*** and ***FQd,*** multiplying them.

So, the management of the loads that present flexibility is carried out by the ***gamma*** variable, which represents how much of the load has been cut:

$$\boldsymbol{gamma} = \begin{matrix}[gamma_1^1 \cdots gamma_{nb}^1 \cdots \\ \cdots gamma_1^{per} \cdots gamma_{nb}^{nper}]^{\boldsymbol{T}}\end{matrix} \tag{18}$$

where:

$gamma_{nb}^{nper}$: factor to cut each flexible load (***FPd***) at bus i and period k.

Related to reactive power for elements connected to the grid via inverters, such as PV systems and BESS, these will be taken as control variables if reactive dispatch is being considered. Otherwise, if the power factor is considered fixed, the reactive power injected by these systems will be a dependent variable.

So, if the reactive dispatch of PV systems and BESS are optimized by the MPOPF, the reactive power injection of PV (***Qgsun***) and the reactive power injection of BESS (***Qbat***) are:

$$Qgsun = \begin{matrix}[Qgsun_1^1 \ldots Qgsun_{nb}^1 \ldots \\ \ldots Qgsun_1^{nper} \ldots Qgsun_{nb}^{nper}]^T\end{matrix} \tag{19}$$

$$Qbat = \begin{matrix}[Qbat_1^1 \ldots Qbat_{nb}^1 \ldots \\ \ldots Qbat_1^{nper} \ldots Qbat_{nb}^{nper}]^T\end{matrix} \tag{20}$$

where:

$Qgsun_i^k$: reactive photovoltaic power injected at bus i and period k and,

$Qbat_i^k$: reactive battery power injected at bus i and period k.

Reactive dispatch of D-FACTS can also be considered a control variable and, thus, be optimized. Its operation will be based on voltage levels, actuating mainly for voltage control. Since the circuit presents different elements that can act to improve the voltage levels, in future analysis they will be considered individually in different scenarios, allowing to verify the effectiveness of each method application (voltage regulator, capacitor bank, reactive dispatch of the generation and storage systems, and the D-FACTS operation):

$$\mathbf{Bst} = [\, Bst_1^1 \;\; \cdots \;\; Bst_{nb}^1 \;\; \cdots \;\; Bst_1^{per} \;\; \cdots \;\; Bst_{nb}^{nper} \,]^{\boldsymbol{T}} \tag{21}$$

where:

Bst_i^k: the susceptance capacitive of D-SVC bus i and period k.

Finally, the active (***Pg***) and reactive (***Qg***) power provided from the substation at bus 1 are:

$$\boldsymbol{Pgh} = [\, Pg_1^1 \;\; \ldots \;\; 0 \;\; \ldots \;\; Pg_1^{nper} \;\; \ldots \;\; 0 \,]^{\boldsymbol{T}} \tag{22}$$

$$\boldsymbol{Qgh} = [\, Qg_1^1 \;\; \ldots \;\; 0 \;\; \ldots \;\; Qg_1^{nper} \;\; \ldots \;\; 0 \,]^{\boldsymbol{T}} \tag{23}$$

where:

Pgh_i^k: active power injected at bus i and period k and,

Qgh_i^k: reactive power injected at bus i and period k.

C. OBJECTIVE FUNCTION

The objective function (OF) proposed for the MPOFP comprehends:

- minimization of the operational costs;
- minimization of battery degradation costs (if a battery system is considered);
- minimization of load deviation of flexible loads and microgrids from the predicted or ideal load (if flexible loads and/or microgrids are considered);
- minimization of power losses.

Operational cost criterion is defined as:

$$foper = wc.\boldsymbol{u}^{\boldsymbol{T}}.\mathrm{c}\,(\boldsymbol{Pg}) \tag{24}$$

where:

wc: weight relative to the importance of the operational costs criterion.

c (***Pg***): energy cost function related to power provided by substation and other generation systems belonging to the power utility. This function also depends on the tariff values considered.

$\boldsymbol{u}$: unit vector with size ($nb.nper$ x 1).

The next criterion is related to battery degradation costs. This should be minimized, once every time that the battery realizes a cycle (charge and discharge), part of its lifetime is lost [31].

According to [32] the battery degradation cost ($cost_{deg}$) can be defined by (25). This proposed model considered the battery bank cost ($cost_{BB}$), the DoD, the expected number of cycles (n_cycles) for the battery over its lifetime, and the total energy storage capacity of the system ($Ebat$). It is important

to highlight that most of these characteristics varies according to system technology, size and type of operation realized.

$$cost_{deg} = \frac{cost_{BB}}{DoD.n_{cycles}.Ebat} \tag{25}$$

With the degradation cost definition is possible to write the corresponding OF criterion in (26).

$$fcost_{bat} = wbat.\boldsymbol{u}^{\boldsymbol{T}}.\mathrm{c}\,(\mathbf{Pbat}) \tag{26}$$

where:

wbat: weight relative to the importance of battery degradation costs criterion;

c (***Pbat***): cost function based on linear cost function $cost_{deg}$.

If a concern that the battery is fully charged at the end of the day, one more optimization criterion can be added to the problem to guarantee only one cycle during the day. This criterion can be added to (27).

$$fcost_{bat} = \mathrm{w}bat.\mathbf{u}'.\mathrm{c}\,(\boldsymbol{Pbat}) + \mathrm{wload}.\mathbf{u}'.\boldsymbol{Pbat} \tag{27}$$

where:

wload: weight relative to the importance of BESS load maximization.

The minimization of load deviation of flexible loads and microgrids is defined as:

$$f_{flexible} = wgd.\boldsymbol{u}^{\boldsymbol{T}}[(\boldsymbol{gamma} - \mathbf{u})]^2 \tag{28}$$

where:

wgd: weight relative to the importance of load flexibility management.

The values of ***gamma*** multiply ***FPd*** and ***FQd*** to decrease the injection or absorption of the predicted load and must deviate minimally from the unit value (which corresponds to the ideal values). As the (***gamma*** - **u**) parcel is squared, the result is positive, and the difference module is always minimized.

Aiming to avoid that the values of ***gamma*** be smaller than 1, which correspond to dispatch less than the scheduled load (***FPd***), one more optimization criterion can be included, which corresponds to maximize the adjusted values of ***gamma***. Therefore, this criterion forces that the total expected load must be supplied, and it is weighted by $w_{targetload}$ coefficient. Adding this new criterion in (28), the $f_{flexible}$ criterion is written as:

$$f_{flexible} = wgd.\boldsymbol{u}^{\boldsymbol{T}}[(\boldsymbol{gamma} - \boldsymbol{u})]^2 - w_{targetload}.\boldsymbol{u}^{\boldsymbol{T}}.\boldsymbol{gamma} \tag{29}$$

At least, the criteria related to power losses minimization is given by:

$$flosses = wp.\boldsymbol{u}^{\boldsymbol{T}}.\mathrm{c}\,(\boldsymbol{Pg} + \boldsymbol{Pgsun} - \boldsymbol{Pd} - \boldsymbol{gamma}.\boldsymbol{FPd} - \boldsymbol{Pbat}) \tag{30}$$

where:

wp: weight relative to the importance of the loss criterion;

c (***Pg*** + ***Pgsun*** − ***Pd*** − ***gamma***.***FPd*** − ***Pbat***): energy cost function. This function depends on the tariff value that is considered according to the case of the study.

With the definition of all the parts of the objective function it is possible to compile the multiobjective function:

$$OF = foper + fcost_{bat} + f_{flexible} + f_{losses} \tag{31}$$

Regarding the values of the weights used to prioritize the parcels of the objective function, it is important to note that the sum of all of them should be equal to one, being the correspondent values decided through exhaustive analysis to choose the best values that meet the planner's interests.

The objective function is restricted to the operational constraints to get its optimum value.

D. OPERATIONAL CONSTRAINTS

The operational constraints are divided into two groups: the equality and the inequality constraints.

1) EQUALITY CONSTRAINTS

The active and reactive power injections are represented as a function of **x** and **a** [21]: $\mathbf{P}(\boldsymbol{x}, \boldsymbol{a})$ and $\mathbf{Q}(\boldsymbol{x}, \boldsymbol{a})$, respectively.

The active and reactive power balance equations are:

$$\boldsymbol{P} = \boldsymbol{Pgh} + \boldsymbol{Pgsun} - \mathbf{diag}\,(\boldsymbol{gamma})\,.\boldsymbol{FPd} - \boldsymbol{Pbat} \tag{32}$$

$$\boldsymbol{Q} = \boldsymbol{Qgh} + \boldsymbol{Qgsun} - \mathbf{diag}\,(\boldsymbol{gamma})\,.\boldsymbol{FQd} - \boldsymbol{Qbat} + \mathbf{diag}\left(\left|\dot{\boldsymbol{V}}\,(\boldsymbol{x})\right|^{\mathbf{2}}\right)(\boldsymbol{Bsh} + \boldsymbol{Bst}) \tag{33}$$

where:

$\left|\dot{\boldsymbol{V}}\,(\boldsymbol{x})\right|$: magnitude of the voltage phasor, which is calculated as a function of vector $\boldsymbol{x}$.

2) INEQUALITY CONSTRAINTS

The inequality constraints consider the physical and operational limits of the system. Equations (34) to (44) represent the range defined for the variables, based on the boundary values aforementioned. All the variables delimited by the intervals are optimized in the MPOPF, so the interval defines the possible values that they can assume to achieve the convergence of the problem.

$$\boldsymbol{Pg}_{min} \le \boldsymbol{Pg} \le \boldsymbol{Pg}_{max} \tag{34}$$

$$\boldsymbol{Qg}_{min} \le \boldsymbol{Qg} \le \boldsymbol{Qg}_{max} \tag{35}$$

$$\boldsymbol{V}^{\mathbf{2}}_{\mathbf{min}} \le \left|\dot{\boldsymbol{V}}\,(\boldsymbol{x})\right|^{\mathbf{2}} \le \boldsymbol{V}^{\mathbf{2}}_{\mathbf{max}} \tag{36}$$

$$\mathbf{F}_{\mathbf{min}} \le \mathbf{F}(\mathbf{x}) \le \mathbf{F}_{\mathbf{max}} \tag{37}$$

$$\boldsymbol{a}_{\mathbf{min}} \le \boldsymbol{a} \le \boldsymbol{a}_{\mathbf{max}} \tag{38}$$

$$\boldsymbol{gamma}\ \mathbf{FPd} \le \mathbf{FPd} \tag{39}$$

$$-\boldsymbol{Bst}_{max} \le \boldsymbol{Bst} \le \boldsymbol{Bst}_{max} \tag{40}$$

$$\boldsymbol{Pgsun}^2 + \boldsymbol{Qgsun}^2 \le \boldsymbol{Ssun}^2 \tag{41}$$

$$\boldsymbol{Pbat}^2 + \boldsymbol{Qbat}^2 \le \boldsymbol{Sbat}^2 \tag{42}$$

$$-\boldsymbol{Ssun} \le \boldsymbol{Qgsun} \tag{43}$$

$$-\boldsymbol{Sbat} \le \boldsymbol{Qgbat} \tag{44}$$

Equations (34) and (35) represent the substation transformer active and reactive power injection limits, respectively. (36) represent the voltage magnitude limits. (37) are related to the power flow limit through the lines. (38) are the boundaries for voltage regulator tap position. (39) are the limits of flexible load management. (40) represents the D-SVC limits. Equation (41) represents the apparent power limit of the solar inverters, and (42) the apparent power of the battery inverters. Equations (43) and (44) present the limit boundaries for the reactive power dispatch when this possibility is allowed for DERs.

For the BESS, the active power limit injection is defined by (45), whereas the energy stored in the battery is limited by (46).

$$\boldsymbol{P_{bat_{min}}} \leq \boldsymbol{Pbat} \leq \boldsymbol{P_{bat_{max}}} \tag{45}$$

$$\boldsymbol{EBAT_{min}} \leq \boldsymbol{Ebat} \leq \boldsymbol{EBAT_{max}}. \tag{46}$$

The effective amount of energy stored ($Ebat_i^t$) depends on the values of energy stored in the previous instants, considering the initial energy at t = 0 (*Earrive*), and the efficiency (eff_{bat}) of the charging and discharging process.

$$Ebat_i^t = \sum_{k=1}^{nper} [Pbat_i^k - (1 - \mathrm{eff_{bat}}) \cdot \left|Pbat_i^k\right|].\Delta t + Earrive \tag{47}$$

where:

Δt: time interval between two consecutive periods.

The problem presented by the equations (31) – objective function, (32) and (33) – equality constraints and, (34) to (47) – inequality constraints, represents the MPFOP model, that is solved by the Primal-Dual version of the Interior Points Method implemented in Python language.

The Interior Points Method obtains the best solution, keeping the search inside the area delimited for restrictions. The inequalities are changed to equality through the introduction of slack variables. Additionally, a logarithmic barrier function is added to the objective function to guarantee the non-negativity of the slack variables. In sequence, the Karush–Kuhn–Tucker (KKT) conditions that express the first optimality conditions of the optimization problem are resolved by the application of Newton's method to obtain the solution of the nonlinear equations (Karush-Kuhn-Tucker optimization base conditions). This method was selected due to its good performance obtained to solve traditional OPF [21], [25].

IV. SYSTEM CHARACTERISTICS

The maintenance of voltage levels inside power quality values is one of the most important characteristics of the power grid. Voltage behavior on distribution grids depends on the active power behavior. So, when the demand in the circuit increases, the voltage tends to present lower values, whereas the greater injection of power increases the voltage.

In Brazil, the procedures for Distribution of Electric Energy in the National Electric System (from Portuguese, PRODIST), define in Module 8 – Electric Energy Quality [33], the bands of voltage for distribution buses when the system is in steady-state, being this values presented at Table 1. The voltage levels need to be kept between 0.93 and 1.05 pu even with the connection of DG, EVs, or BESS systems. For this purpose, equipment as voltage regulators (VR), capacitor banks, and D-FACTs are placed along the feeder, as well as the contribution of reactive dispatch from PV and BESS systems could be considered.

TABLE 1. Classification of voltage levels.

$\mathbf{0.93 \leq V \leq 1.05\ pu}$	Adequate
$\mathbf{0.90 \leq V < 0.93\ pu}$	Precarious
$\mathbf{V < 0.9\ or\ V > 1.05\ pu}$	Critical

The provisioning of reactive power by elements connected to the grid by inverters can be considered an ancillary service since it can be requested and remunerated by the DSO if there is regulation and a defined market for it.

To calculate the operational cost for the DSO, the white tariff values were considered. In 2019, according to COPEL distribution power utility, the values for this tariff for residential consumers [34] were: 0.081426 USD/kWh for off-peak hours (*hfp*), 0.111261 USD/kWh for pre-and post-peak hours (*hpp*) and 0.172793 USD/kWh for peak hours (*hp*).[1] As these tariff values will be used to calculate the grid operation cost, the values without taxes were adopted.

The *hfp*, *hpp*, and *hp* values compose the vector ***aah*** with dimension (*nb.nper* x 1) that indicates the tariff for each hour, and this behavior is illustrated in Fig. 1.

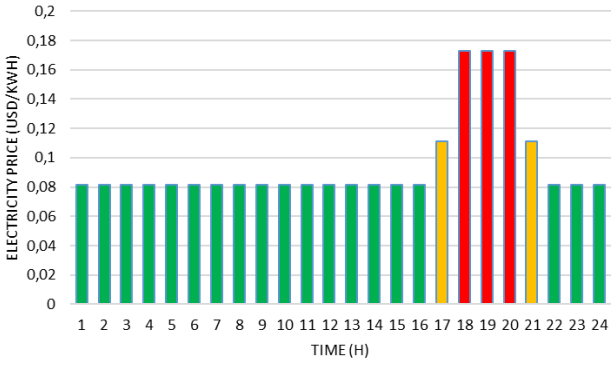

FIGURE 1. Brazilian white tariff values and behavior.

For the distributed generation with PV systems, different radiation behaviors can be considered, however, as it is desired to study the most critical scenario, the analysis for clear sky days was prioritized, resulting in the maximum solar radiation. Fig. 2 illustrates the radiation profile that was considered, being obtained from measurements realized at Curitiba city, in Brazil.

[1]The conversion of values from Brazilian Reais (BRL) to American Dollars (USD) was carried out based on the exchange data of April 26, 2021, according to the Brazilian Central Bank: 1USD = 5.4560 BRL.

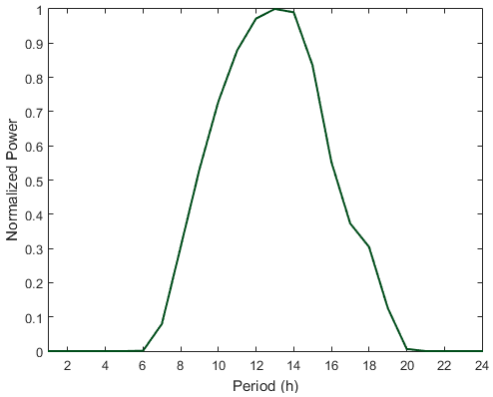

FIGURE 2. Solar irradiation profile.

A. TEST CIRCUIT

The first circuit that was analyzed was a test feeder with 90 buses adapted from [35], [36]. This circuit was based on [37] system of 69 medium voltage (MV) buses, in which were added 20 low voltage (LV) buses. The schematic diagram of the distribution grid is presented at Fig. 3.

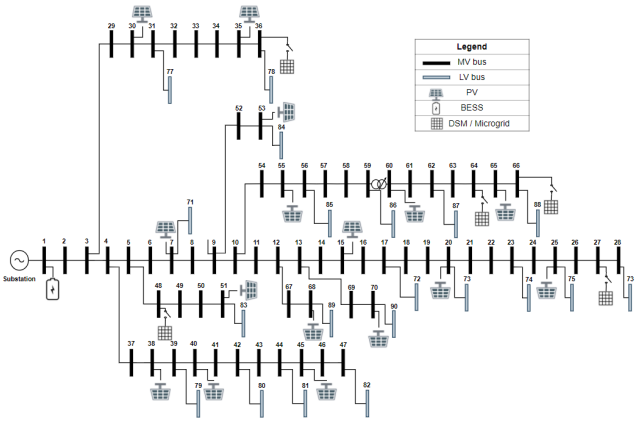

FIGURE 3. Test distribution system with 90 buses.

The distribution system presents a voltage regulator placed between buses 59 and 60, since lower voltage levels are seen at LV buses 86, 87, and 88. The VR consists of an autotransformer with 32 different tap positions with +/- 10% of voltage control for each tap level. Usually, VR placed outside of the substation bus is defined in a fit-and-forget configuration. However, as an ADN scenario is being considered, it was assumed that this equipment can present an automatic control, similarly to an online tap changer voltage regulator (OLTC) and will adjust the tap positioning according to grid necessities.

There are also five fixed capacitor banks with commercial values of 100, 200, and 300 kvar, placed at buses 13, 23, 37, 57, and 62. These capacitor banks are fixed, being considered connected or disconnected during the entire period of study, according to the ongoing analysis.

As the study considers an ADN, DERs are placed on it, as illustrated in Fig. 3, being those characteristics described in detail in the following subsections. The study time horizon considered is 24 hours, discretized into 1h.

From 90 buses, 69 are load buses that totalized 4.575 MW of installed load. Regarding the behavior of the loads, the profile sampled in Fig.4 was defined, which is normalized, meaning that it presents values between 0 and 1, being multiplied by the load power installed in each bus. In this way, all the load buses present the same behavior profile, but different values among themselves. Fig.4 shows the behavior of the active and reactive power of the loads, which present a power factor of 0.92.

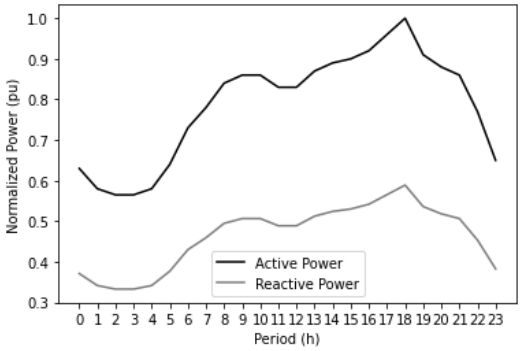

FIGURE 4. Load active and reactive power profile for 90 bus test feeder.

Regarding PV system connection, 16 distributed generation systems were placed on it [36]. All systems have the same installed power and same generation profile behavior. The total installed power of the PV systems totalizes 3.2025 MW, corresponding to a penetration level of 70% concerning the total installed load [25].

For the power factor of PV system inverters, three different options were considered: unit power factor, which corresponds to injection of only active power; fixed power factor, which requires the injection of reactive power from PV systems; and the reactive power dispatch, being the power factor variable, allowing the provisioning of voltage support as an ancillary service with reactive power injection according to grid necessity.

For the electric mobility there are six electric vehicle chargers of 7.4 kW and three of 22 kW installed along with the distribution system, totalizing 110.4 kW of installed power. The EV chargers of 7.4 kW were connected to low voltage buses 72, 74, 78, 82, 88, 90, whereas the 22 kW systems were connected to medium voltage buses 51, 53, and 65.

The average energy storage capacity of the vehicles was taken as 30 kWh, and the initial state-of-charge of the battery from EVs when they arrive at the charging station was considered as 20% (corresponding to a depth-of-discharge of 80%) and resulting in a demand of 24 kWh.

According to [38], most of the charging of electric vehicles takes place at night, due to lower tariffs. The second most frequent charging time corresponds to the period when people are working and are not using the vehicle. Therefore, two different charging behaviors were considered: night charging (from 0:00 to 6:00) which totalizes a power demand of 662.4 kWh, being able to charge 27 vehicles with the before mentioned characteristics; or day charging (from

9:00 to 18:00), totalizing 993.6 kWh, able to charge 41 vehicles in the same conditions previously defined. The behavior of both charging strategies along the day is presented in Fig. 5.

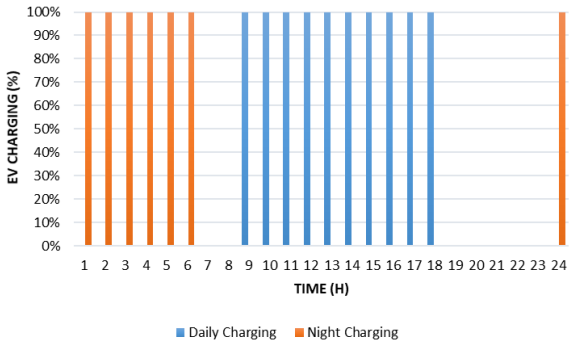

FIGURE 5. EV daily and night charging behaviors.

The medium voltages buses that receive the EV chargers also present solar generation installed, resulting in a similar behavior of a carport system (generation and EV consumption in the same point of the system). The demand profile of EV chargers is included in vector ***Pd***.

In the present work the definition of the placement of the EV chargers was done arbitrarily, however, as a suggestion for future works, the optimization of their placement can also be done.

The battery energy storage stationary system modeled for the simulations corresponds to a lithium-ion battery with 1MW/2MWh. Based on market data this battery would cost approximately 2.2 million dollars.

In terms of operational characteristics, the BESS will present a maximum DoD of 70%, which means approximately 4,000 cycles to failure.

Another important characteristic to be considered is the efficiency of the charging and discharging process. According to [39] lithium-ion batteries present efficiency higher than 90%, low self-discharge rates, and are not affected by the memory effect as other energy storage technologies. In this way, the 90% value was considered for the efficiency of both charge and discharge processes.

As aforementioned, the battery is connected to the power grid using an inverter. Thus, two different scenarios were considered for the power factor, being first the fixed value of 0.92 and after allowed the reactive power dispatch, also aiming to use reactive power to improve distribution grid voltage levels.

Concerning the location of the BESS, two possibilities were also considered. As the system will be an equipment of the DSO, it can be placed at the substation bus, reducing costs related to space rental and investments in control and communication systems, however, the benefits provided by the system can be limited, as will be shown in the results section. Another possibility could be the placement outside of the substation bus. In [25] different allocations were evaluated, and one of the best results is achieved when the BESS is connected to bus 8, since major part of the total load (66.15%) is located downstream of this point.

The D-SVC has its reactive power injection dispatchable according to the grid needs. This equipment was installed at a bus in which there was a capacitor bank (bus 57), since at that point tends to have voltage problems. Additionally, it was desired to analyze the complementarity of voltage regulator operation and the D-FACTS. The other capacitor banks remain fixed and with the same values.

For the circuit simulated, flexible loads were considered at buses 27, 36, 48, 64, and 66. The range of load variation is defined at restriction (39), and it is considered the possibility to vary up to 15% of the demanded power. It is important to highlight that the DSM can happen only if some operational constraint is reached and is not allowed to be performed based on grid operational cost reduction.

The power grid can present not only one microgrid (MG) but multiple microgrids placed along the feeder simultaneously, resulting in different interactions with the main grid.

For the test circuit, MGs were allocated in place of flexible loads (buses 27, 36, 48, 64, and 66). Regarding the behavior of the microgrids over 24 hours, three distinct periods of operation were considered: 0h to 7h corresponds to load (the price of grid energy tends to be lower during this period since there is less demand), 8h to 17h is disconnected from the grid (taking advantage of existing generation in the MG itself for supplying internal loads), 18h to 21h delivers power to the grid (performing power injection in the hour of higher demand in the distribution grid), 22h to 23h returns to operate as load, absorbing power from the main grid.

B. REAL CASE OF DISTRIBUTION SYSTEM

Another circuit was simulated with the MFOP proposed, but now corresponding to a real distribution system from Curitiba, Paraná, Brazil. This feeder presents 2,119.08 kW of installed power, of which 38% corresponds to low voltage consumers and 62% to medium voltage consumers and it has 359 buses and 358 lines. The drawing of the feeder is illustrated in Fig. 6.

From Fig. 6 legend *ssdbt* means low voltage lines; *ssdmt* are medium voltage lines, *sub* corresponds to the substation; *ucbt* is the low voltage consumers; *ucmt* are medium voltage consumers; *unsemt* are medium voltage switches, and *untrd* are distribution transformers that connect LV to MV (there are a total number of 64 in the circuit).

For the load profile, real data information was used in the correspondent scenarios of summer and winter. Analyzing the load data of an entire month, the mean value and the standard deviation around the mean are represented in Fig. 7 for summer and in Fig. 8 for winter. Those profiles were normalized and applied for all load buses in the circuit.

Additionally, to the load profile analysis, the energy consumption values were also evaluated, allowing the definition of a load utilization factor in order that the total energy consumption of the simulated month presents the same value of the real measurements. For the summer months the energy

FIGURE 6. Real distribution feeder.

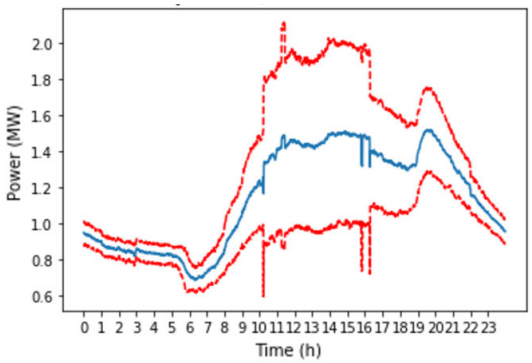

FIGURE 7. Active power profile for real distribution feeder for summer, being the filled line the mean and the dashed line the standard deviation around the mean.

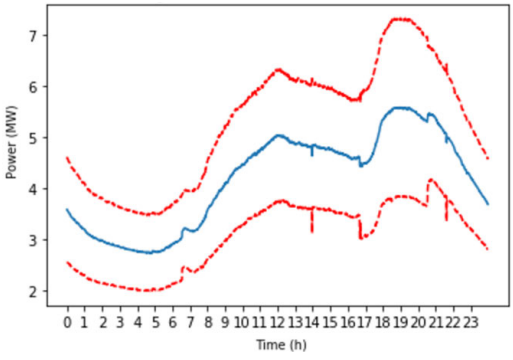

FIGURE 8. Active power profile for real distribution feeder for winter, being the filled line the mean and the dashed line the standard deviation around the mean.

consumption in the feeder is 27 MWh/day and for the winter it is 100 MWh/day.

Following Brazilian grid characteristics, circuit voltage levels are 220/127 V for LV and 13.8 kV for MV, and the frequency is 60 Hz.

Another important characteristic of the real distribution system is related to the voltage level at the substation bus. Following the technical norm NTC 905100 of Paraná State Power Utility - COPEL [40] the substation voltage should change according to the demand level of the circuit, presenting the values defined in Table 2.

TABLE 2. Substation voltage values according to load levels.

Load Stage	Minimum Voltage (pu)	Maximum Voltage (pu)	Period
Heavy	0.9927	1.00	18h00 – 22h00
Intermediate	0.9783	0.9927	08h00 – 17h00 23h00 – 00h00
Low	0.9565	0.9783	00h00 – 07h00

This feeder does not present any voltage regulator, capacitor bank, or D-FACTS allocated, not even DG or BESS.

In the context of the Research and Development (R&D) project PD-02866-0511/2019, a real microgrid was connected to this feeder, working as a pilot project connected to the distribution feeder. This microgrid is placed at Barigui Park, which is the largest public park in Curitiba City, and is composed of photovoltaic solar generation, battery energy storage, flexible loads, and a carport system.

To evaluate its integration with the real distribution feeder, the MPOPF methodology presented in this paper will be integrated in a hierarchical way of control, communicating with microgrid internal optimization control. It will be considered different operational schedules for MG, being evaluated in two different seasons: summer and winter, illustrated in Fig. 9 and 10, respectively.

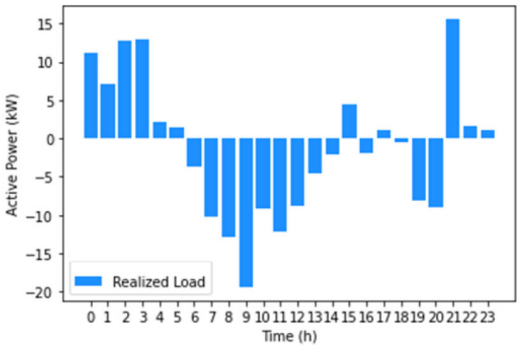

FIGURE 9. Typical active power schedule for the MG in summer.

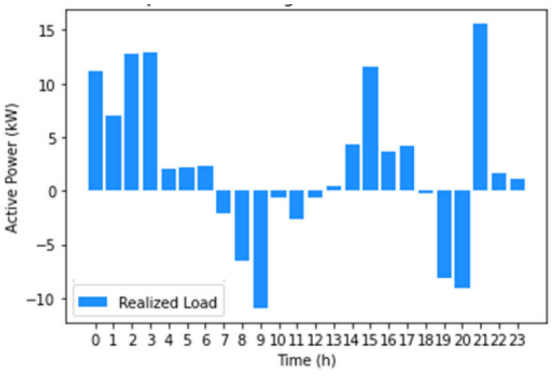

FIGURE 10. Typical active power schedule for the MG in winter.

In addition, for the present study, the distribution grid will be transformed into an ADN, with solar DG penetration and the placement of a BESS system. It is important to highlight that these elements aggregated on the grid for the study will be modeled in the same way that was previously done for the 90 buses test feeder.

Regarding the MPOPF execution, aiming to improve the computational time, especially for the real feeder, a new strategy was proposed, as illustrated in Fig. 11 flowchart. As the real feeder has many buses (a total of 359 buses), and the matrices are sized as *nb.nper*, the computational time spend to build these matrices is high. Since that some of the matrices building only depends on the graph characteristics of the circuit, a pre-processing was defined, resulting in the storage of the matrices. For the different scenarios, only the optimization process needs to be executed. So, getting access to the pre-defined matrices, the optimization can be processed much more quickly than when the matrices organization is considered inside of the entire process. The computational times to run these simulations will be presented in section VI.

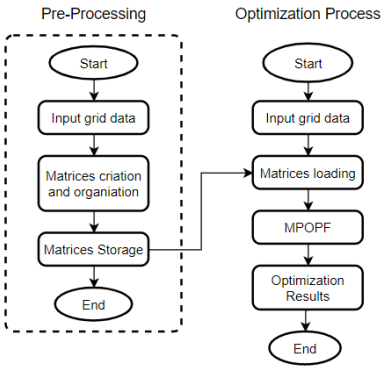

FIGURE 11. Flowchart of new strategy of MPOPF divided into pre-processing and optimization process.

V. 90 BUS TEST FEEDER SIMULATION RESULTS

For the test circuit, the gradual implementation of elements in the distribution grid was performed to verify how the insertion of the elements impacts the power system operation when MPOF is calculated. All combinations of elements that can be allocated in the network were considered and simulated, been the most relevant ones discussed in the sequence.

A. 90 BUS TEST FEEDER – BASE CASE

The base scenario consists of the 90-bus test feeder only with load allocation, corresponding to a classic distribution circuit without any DER. In this case, the voltage regulator (VR) and the fixed capacitor banks were considered, and the total energy demand totalizes 81.27 MWh. In Fig. 12 the active power flow balance from the substation bus is presented, being the reactive power balance illustrated in Fig. 13.

From Fig.12 it is possible to visualize that all load is supplied by the substation. The same happens for reactive power in Fig.13, being, in this case, part of reactive power

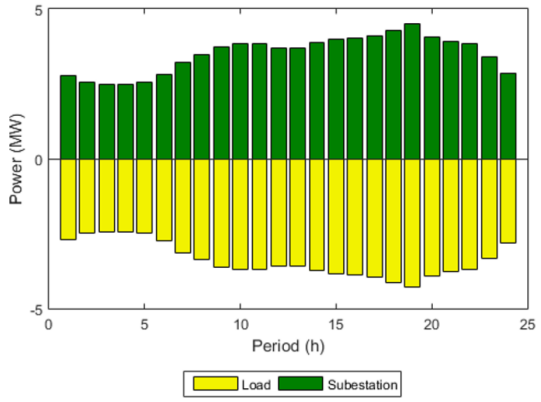

FIGURE 12. Active power balance at the substation bus for 90 buses test feeder base case.

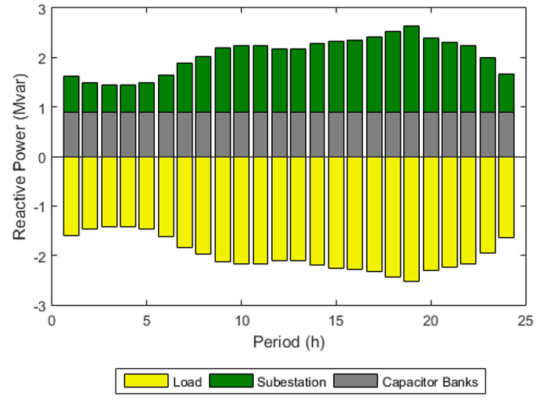

FIGURE 13. Reactive power balance at the substation bus for 90 buses test feeder base case.

demand supplied by fixed capacitor banks and part provided by the substation.

In this scenario, all buses present voltage values inside of the limits to be considered adequate, as shown in Fig.14. The minimum voltage in this circuit is founded at bus 86, however, it is not an undervoltage (it is not under 0.93 pu). In terms of maximum voltage boundary, none of the buses reached these values as well.

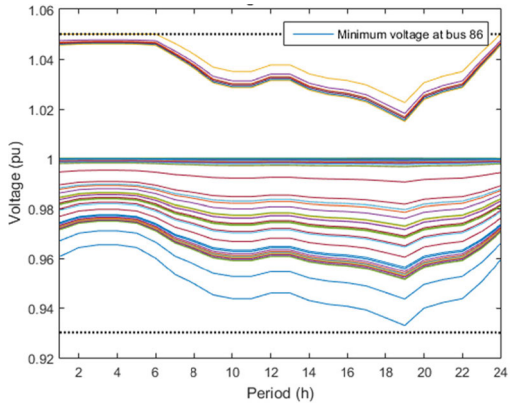

FIGURE 14. Voltage behavior for all 90 buses in base case scenario.

For this scenario, the power losses on the circuit totalize 2.71 kWh (3,33%), arising from the circulation of power

through the circuit lines. Concerning the operational cost of the DSO to supply all the load, it totalizes 8,122.75 USD.

Regarding the VR tap operation, the results are presented in Fig.15, in which it is seen that the regulator needs to change its tap position during the day to avoid undervoltage since it operates in maximum position (tap = 1.1) during most of the day.

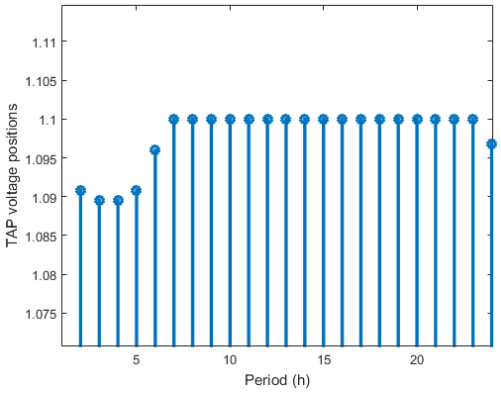

FIGURE 15. Voltage regulator tap changes for 90 buses base case scenario.

B. CHANGING VOLTAGE SUPPORT EQUIPMENT

In the sequence, some changes in voltage support equipment were considered. First, the VR was removed and only the capacitor banks were considered, after, the opposite was done, being removed the capacitor banks, and being considered just the VR operation. In both cases, undervoltage were founded along the feeder, mainly in the branch where the VR is located.

In terms of power losses, for both cases, the values increased (3.45% and 3.96% respectively), being this effect reflected on prices since, with more losses, more power needs to be provided by the substation bus.

Assuming the allocation of the D-SVC at bus 57, in place of the fixed capacitor bank previously existing at this bus, the possibilities of removing either the voltage regulator or the fixed capacitor banks were considered. However, when VR is removed and it is considered only the D-FACTS and fixed capacitor banks for voltage support, the grid presents undervoltage problems, whereas for the scenario with VR and D-SVC the grid can operate within proper voltage limits along all buses.

C. INCLUDING DISTRIBUTED GENERATION

Considering the insertion of the distributed photovoltaic generation systems in the grid, an increase in the feeder loading level was also assumed, to evaluate the grid behavior in a higher load situation. In this way the daily demand for the feeder became 86.47 MWh.

Initially, the operation of PV systems was considered with fixed unity power factor. When this scenario is considered, there are no voltage violation problems in the grid. The power losses were reduced to 2.71% and the operating costs were reduced to 6,560.32 USD, because part of the demand is supplied by the PVs, reducing the demand for power provisioning by substation, as well as the reduction of the power flow in the lines since the DG systems are located close to the loads.

Monitoring the load flow behavior in the buses it can be observed that there is reverse flow in some regions of the feeder. This reverse power flow is absorbed by the loads located nearby and does not reach the substation bus. Fig. 16 presented the reverse power flow values in each bus at 12h (time of the peak of solar generation).

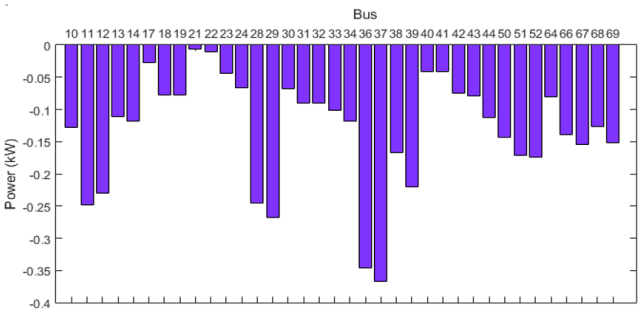

FIGURE 16. Buses with reverse power flow for 90 buses test case with DG at 12h.

In the sequence is considered the PV system inverters operation in a four-quadrant model with reactive power dispatch. In Fig. 17 is presented the reactive power injection profile for all DG systems. Some systems begin to inject reactive power into the system during peak load hours and perform lower injections during the period of higher active generation in the PV, since both injections are limited by the apparent power capacity of the inverter.

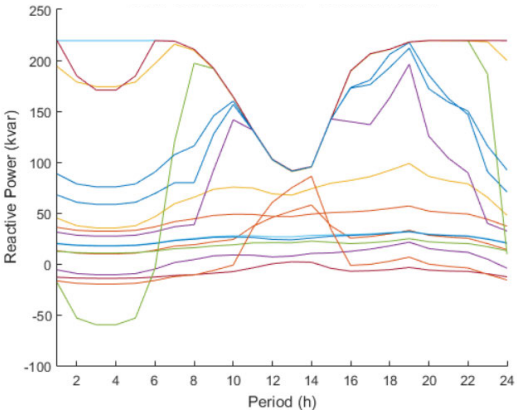

FIGURE 17. PV systems reactive power dispatch.

When reactive dispatch happens, it is possible to operate the grid using only VR or fixed capacitor banks. However, it is important to emphasize that, in this work, PV systems owners have no benefit from contributing to the reactive dispatch of the grid.

In the scenario with reactive power dispatch, it was also obtained the reduction of power losses, being 2.26%, and a total operational cost of 6,519.98 USD (when operating in

conjunction with VR and the previously existing capacitor banks in the grid).

The voltage behavior for all buses with the reactive power dispatch from the PV systems is presented in Fig. 18. In this case is visible the increase of voltage levels during solar generation, due to the increase of active power provisioning and load supplied locally. During load peak time, there are no undervoltage in the circuit and the minimum voltage levels are higher than in the scenario without DG (Fig. 14).

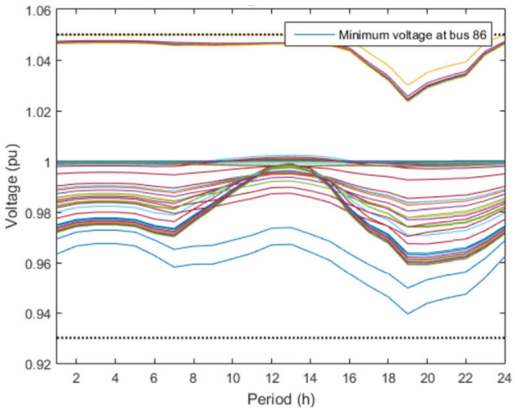

FIGURE 18. Voltage behavior for all 90 with 70% of distributed generation penetration and reactive dispatch.

Assuming that distribution grid could have 100% of DG penetration (which corresponds to the same DG and load installed power), there is a tendency to have problems with overvoltage at peak solar generation time, mainly because it does not coincide with the peak load of the feeder.

Running the simulation for this case, and do not considering the D-SVC and reactive dispatch from PVs, it is obtained the convergence of the problem, however, the voltage behavior presents some problems. To keep voltage levels inside of acceptable levels, the substation bus presents 1.05 pu almost all day, and for the period with high solar generation levels, its voltage quickly changes to 0.98 pu, as shown at Fig. 19, aiming to avoid overvoltage. With this voltage variation at the substation bus, all circuit buses present the same behavior and the entire circuit buses have high voltage changes due to the massive insertion of DG (Fig. 20).

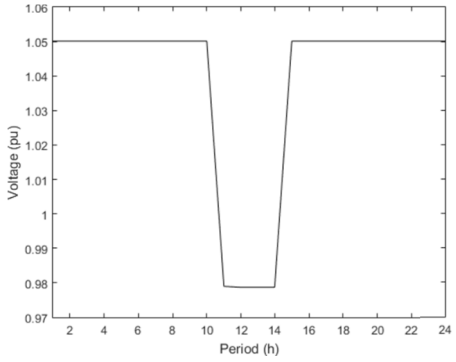

FIGURE 19. Substation bus voltage behavior for 100% PV penetration with no D-SVC and no reactive dispatch.

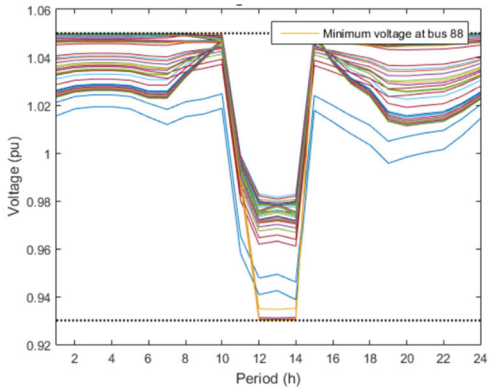

FIGURE 20. Voltage behavior for all buses for 90 buses test feeder with 100% PV penetration with no D-SVC and no reactive dispatch.

In addition to the voltage variation at the substation bus, VR acts by reducing the TAP values during the solar generation period to avoid voltage problems in the downstream buses (Fig. 21).

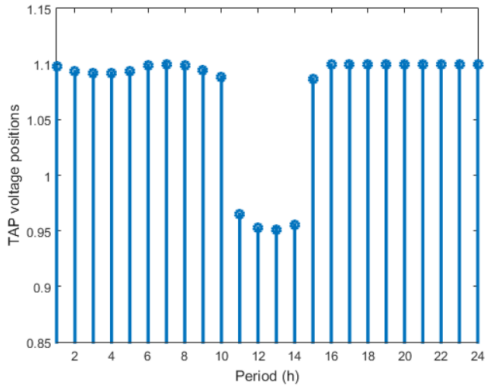

FIGURE 21. Voltage regulator tap changes for 90 buses test feeder with 100% of PV penetration and no D-SVC and no reactive dispatch.

Including the D-SVC operation, it is possible to consider 100% of penetration with smooth voltage changes on the circuit, keeping all voltage buses inside of the adequate range. At the substation bus behavior, presented in Fig. 22, it is seen a lower voltage variability, being most of the day at 1pu and going to 0.98 pu during the solar generation period.

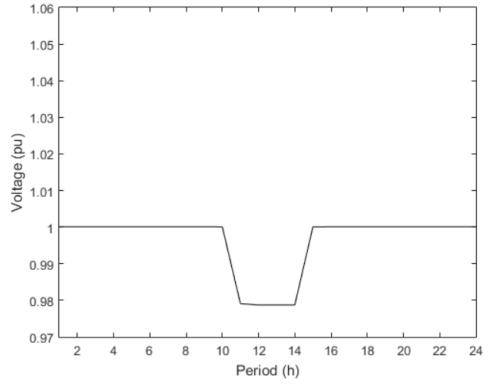

FIGURE 22. Substation bus voltage behavior for 100% PV penetration with D-SVC and no reactive dispatch.

In addition, the D-SVC changes its operation and starts absorbing reactive power during the period when there is an excess solar generation on the feeder (Fig. 23).

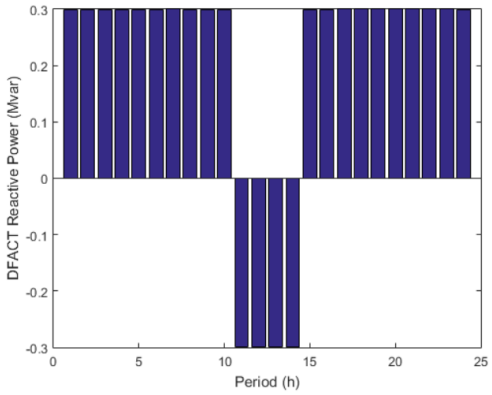

FIGURE 23. D-SVC behavior at 90 buses tests feeder with 100% of PV penetration without reactive dispatch.

Assuming the PV inverters with four-quadrant mode, some of these systems will start to absorb reactive power during the period of higher solar generation, as shown in Fig. 24, contributing to mitigating possible overvoltage violations and allowing greater accommodation of DG systems on the grid. With the reactive injection/absorption from the inverters, the D-SVC operation is modified and starts to happen gradually throughout the day (Fig. 25).

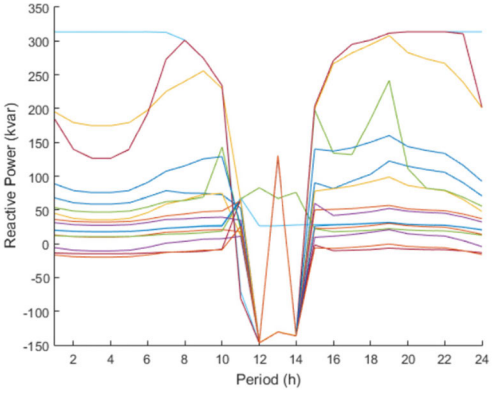

FIGURE 24. PV systems reactive power dispatch with 100% penetration.

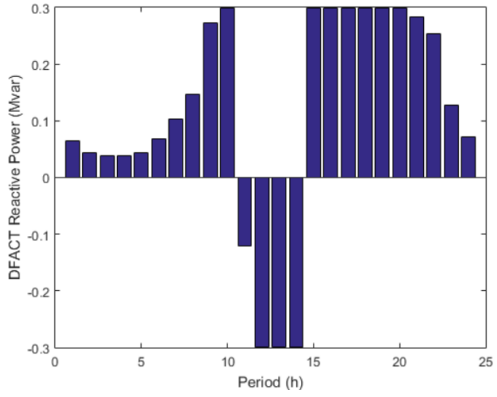

FIGURE 25. D-SVC behavior at 90 buses test feeder with 100% of PV penetration with reactive dispatch.

For the scenario with PV generation and reactive power dispatch in addition to D-SVC operation, the voltage behavior of all buses is presented in Fig. 26. In this case, there is still a decline in voltage levels, but not so strong as visualized in Fig. 20 when there is no reactive power provisioning.

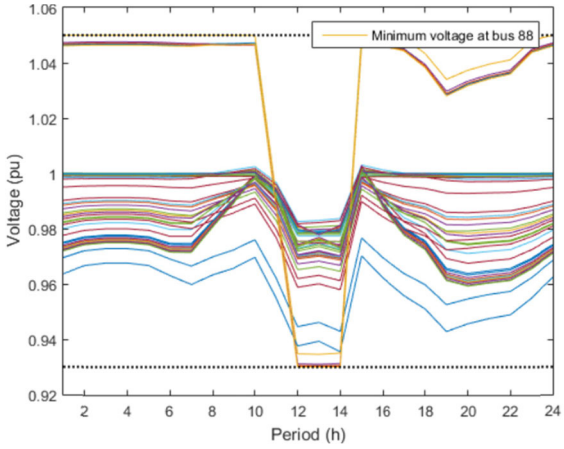

FIGURE 26. Voltage behavior for all 90 buses with 100% of distributed generation penetration and reactive dispatch.

Table 3 presents the comparison between the scenarios with PV systems integration to the distribution network. In the scenarios with 70% of penetration, as much reactive power provisioning is considered lower are the power losses, since it is possible to increase the active power generation and load supplying locally, without voltage violations, and thus reduce the power that comes from substation through the lines to the loads.

TABLE 3. Results after the allocation of PV system.

Scenario	Power Losses	Operational Costs (USD)
70% PV (pf=1)	2.71%	6,560.32
70% PV (RD)	2.26%	6,519.98
70% PV (RD) + D-SVC	2.19%	6,547.70
100% PV (pf=1)	2.16%	5,640.60
100 % PV (pf=1) + D-SVC	2.07%	5,662.26
100 % PV (RD) + D-SVC	2.09%	5,654.90

* RD: Reactive Dispatch

With the D-SVC operation it was possible to get even lower losses and costs, since with reactive power provisioning by the D-FACTS, the inverters of DGs can provide less reactive and more active power to the system, regarding the apparent power limitation. Additionally, all loads can be supplied by distributed generators during part of the day, so no power needs to be provided by the substation, which contributed to costs reduction.

With a 100% penetration of distributed generation, there is reverse flow at the substation bus, which for real circuit applications can result in problems in the settings of control and protection equipment. Fig. 27 shows the reverse power flow at the substation bus at 12h.

For all next scenarios will be considered the distributed generators penetration level of 70%, which corresponds to

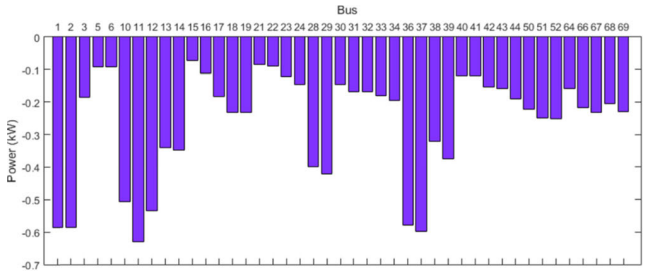

FIGURE 27. Buses with reverse power flow for 90 buses test feeder with 100% of PV penetration at 12h.

high penetration, and allows the evaluation of the largest number of possible scenarios with the placement of other equipment.

D. INSERTING ELECTRIC VEHICLES

With the insertion of electric vehicles (EVs) chargers on the grid, when nighttime charging is considered, the impact on grid operation is lower, since the load increase happens during the feeder's light load period. In addition, it is verified that the grid operation costs are also lower due to the behavior of the applied tariff.

Yet, when daytime charging is considered, the load increase on the feeder occurs at the time of solar generation, which contributes to the reduction of reverse power flow within the feeder, also reducing losses. By comparing the grid operation costs with the entry of daytime charging of EVs there is only a 2% increase in operational costs.

When considering the reactive dispatch of the PV systems, there is a significant improvement in the voltage profile when considering the daytime charging of the EVs. If D-SVC is introduced in this scenario, the voltage profiles present higher values, with the minimum voltage value being 0.935 pu for bus 86, and no voltage values lower than 0.95 for the other buses. Regarding overvoltage, this does not occur in any case.

With the operation of D-SVC, the losses in the circuit decreased 8% in comparison with the scenario where there is only the dispatch of reactive power from the PVs. It is also observed that most of the reactive power is supplied by the PV systems throughout the day, with a reduction in the supply during solar generation, as shown in Fig. 28, due to the apparent power limit of the inverters.

E. INSERTING BATTERY ENERGY STORAGE SYSTEMS

Returning to the grid structure with only photovoltaic systems (unit power factor), the battery storage system was included, being initially placed at the substation bus (with the power factor set at 0.92).

Considering this application, the BESS will operate in a load shedding mode, doing its charging during the period of solar generation. At this time, it has load relief at the substation bus, and the discharge occurs during the peak load period since this is the most expensive time for the system, and the one that tends to present the greatest amount of problems in the operation due to the demand growth. This

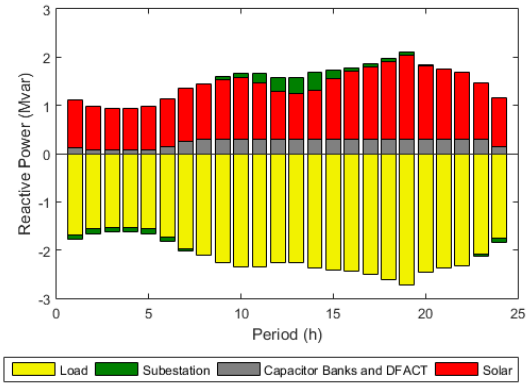

FIGURE 28. Reactive power balance at the substation bus for 90 buses test feeder with PV, EV charging at daytime, and D-SVC.

behavior is presented in Fig. 29, with the power profile realized by the BESS. In Fig. 30 the State-of-Charge (SOC) of the battery at each time is presented, being demonstrated that it charges until reaches its full capacity (100%) and discharged regarding the maximum DoD (70%).

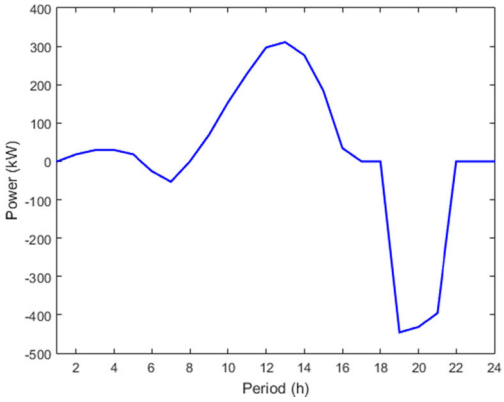

FIGURE 29. BESS active power behavior when connected at the substation bus.

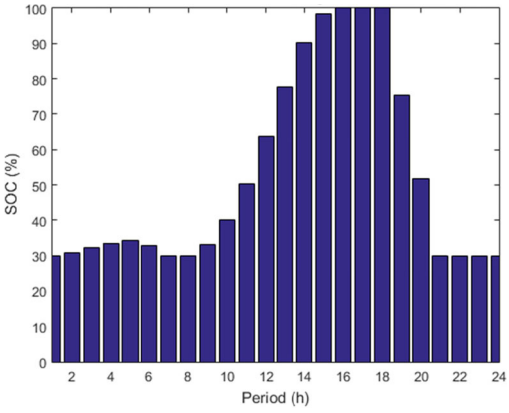

FIGURE 30. BESS State-of-Charge (SOC) when connected at the substation bus.

For this scenario, the grid operational costs were 6,459.83 USD which are added to the depreciation costs of the storage system, which corresponds to 1,177.92 USD. As for losses,

the values obtained were the same as in the scenario with the only DG with unity power factor. This happens since with the battery allocated at the substation bus there is no difference in the power flow that flows through the lines until it reaches the loads.

Considering the possibility of reactive dispatch only by the battery system, with the system allocated at the substation bus there are no operational benefits to the grid.

Changing the positioning of the BESS in the grid and allocating it at bus 8, it was possible to reduce costs and losses since the BESS is close to the loads. Besides performing the load-shedding function, the storage system also contributes to voltage regulation, especially when considering the system's reactive dispatch, being one more equipment capable of supply/absorb reactive power according to the grid needs. With the application of reactive dispatch by the battery, it is verified that, in terms of losses and costs, the D-SVC does not present significant improvements, as well as when verified the behavior of voltage levels. These results are compared in Table 4.

TABLE 4. Results after the allocation of BESS at bus 8.

Scenario	Power Losses	Operational Costs (USD)	Battery Degradation Costs (USD)
PV (pf=1) + BESS (pf=0.92)	2.56%	6,454.90	1,180.17
PV (pf=1) + BESS (RD)	2.47%	6,447.02	1,179.91
PV (RD) + BESS (RD)	2.23%	6,423.85	1,179.25
PV (RD) + BESS (RD) + D-SVC	2.22%	6,424.99	1,179.25

* RD: Reactive Dispatch

For the simulations with batteries, it is seen that the optimization process realized by the MPOPF needs more iterations to reach convergence, going from an average of 10 iterations for the simulations without BESS to 25 iterations with the insertion of the BESS, since it needs to optimize the charging and discharging process as well as the usage of stored energy.

F. INSERTING FLEXIBLE LOADS

To consider the operation of flexible loads, an increase in the feeder loading level was considered, so the operational restrictions can be reached, therefore, a load shedding will be necessary.

Considering the network with PV (pf = 1) and the new load, it was possible to reach the convergence of the optimization process when load shedding is performed at the buses that present this functionality. The highest demand reduction happened at bus 64, since the downstream bus 86 is the most prone to undervoltage.

Avoiding load shedding it is possible to perform load shifting when part of the load was changed from peak time to periods with lower demand in the grid. This behavior is illustrated in Fig. 31, where the load demand at bus 64 is changed from peak time and distributed along the day, totalizing the same daily energy consumption.

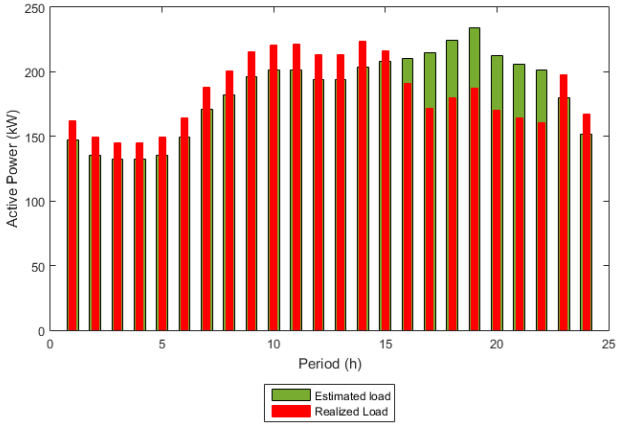

FIGURE 31. Difference between estimated and realized load profiles at bus 64 with DSM.

With load shifting availability and reactive dispatch from BESS and PVs it is possible to reduce the amount of load that is shifted, as well as reduces power losses and operational costs (2.6% of cost reduction). Moreover, improvements in the voltage levels are obtained, with the minimum voltage happening at bus 86 with 0.94 pu, and for all other buses, the minimum voltages reached 0.95 pu.

G. INSERTING MICROGRIDS

Presuming the operation of microgrids in placement of flexible loads, as aforementioned in section IV.A, when the power grid presents only load and PV generation, it is possible to get the optimization convergence without changes in the proposed operation of the microgrids (Fig. 32). For this scenario, the operational costs reduced, since there is low load in the main grid, due to the disconnection of the MGs during part of the day, besides the provisioning of power from the MGs to the grid during the peak period.

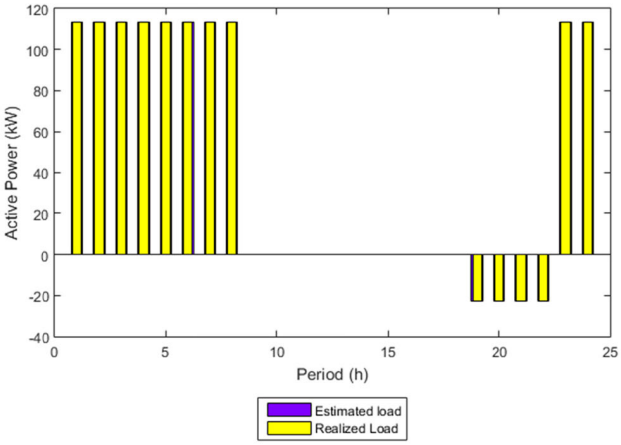

FIGURE 32. Estimated and realized load profiles for the microgrid placed at bus 64.

Assuming the possibility of a load increase in the feeder or even in the microgrids, it could be necessary to propose a new behavior for the MGs to ensure a safe operation of the distribution grid. In this case, it is up to the DSO to inform the expected profile for the internal control of the MGs allowing the provisioning of a new operation plan to be run with the MPOPF, as shown in Fig. 33.

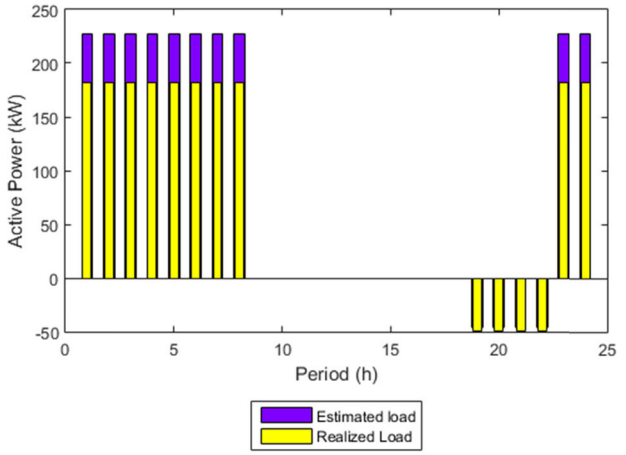

FIGURE 33. Estimated and realized load profiles for the microgrid placed at bus 64 after the MPOPF load shedding, resulting in a proposition of a new MG profile (yellow).

The network behavior was evaluated with the insertion of multiple microgrids, and the previously tested equipment was gradually associated. The results regarding losses and costs are presented in Table 5.

TABLE 5. Results from different scenarios after gradually equipment connection.

	Scenario	Power Losses (%)	Operational Costs (USD)	BESS Degradation Costs (USD)
1	MG + DSM + PV (pf = 1)	1,37	6,258.65	-
2	MG + DSM + PV (RD)	1,29	6,250.92	-
3	MG + DSM + PV (pf =1) + BESS (RD)	1,33	6,161.40	1,174.58
4	MG + DSM + PV (RD) + BESS (RD)	1,23	6,155.65	1,174.36
5	MG + DSM + PV(RD) + BESS (RD) + DFACTS	1,22	6.155,54	1,174.36
6	MG + DSM + PV(RD) + BESS (RD) + DFACTS + VEs	1,29	6,260.82	1,174.35
7	MG + DSM (load shifting) + PV(RD) + BESS (RD) + DFACTS + VEs	2,00	6,310.32	1,172.90

* RD: Reactive Dispatch

For scenarios 1 to 6, from Table 5, it was considered only the possibility of load shedding of the MGs by the DSM, resulting in a total demand of 84.74 MWh for scenarios 1, 2 and 3, 87.74 MWh for scenarios 4 and 5, 85.85 MWh for scenario 6 and finally 86.42 MWh for scenario 7, which present load shifting realized from DSM of the MGs. This variation in daily demand values is a result of the proposed load shedding percentage for each of the scenarios. With the connection of D-SVC, it was possible to increase load supplying and still obtain the lowest percentage levels of circuit losses.

With the entry of EVs, and therefore the increase in the unmanageable load, it was necessary to cut part of the microgrid load, resulting in lower demand throughout the day. In the last scenario, however, with the possibility of load shifting, it was possible to increase the demand supplied compared to scenario 6 since, instead of cutting the load of the MGs, it was proposed to shift them.

The most interesting results came from scenario 7, in which all equipment is considered connected to the grid simultaneously, requiring lots of decisions from the MPOPF. In this way, the following figures present some results from this scenario. Fig. 34 and 35 present the active and reactive power balances at the substation, respectively.

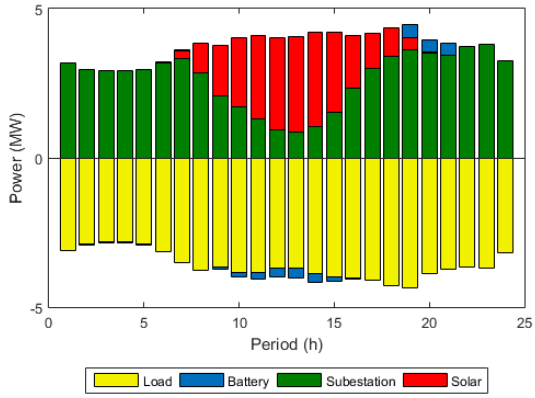

FIGURE 34. Active power balance at the substation bus for 90 buses test feeder at scenario 7.

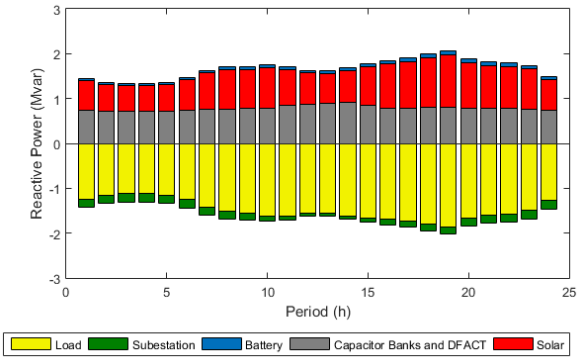

FIGURE 35. Reactive power balance at the substation bus for 90 buses test feeder at scenario 7.

From Fig. 35 it is visible the operation of D-SVC in addition to fixed capacitor banks since its behavior varies along the day, being detailed in Fig. 36. With the possibility of reactive dispatch from many types of equipment,

the substations started to absorb part of the reactive power through the system.

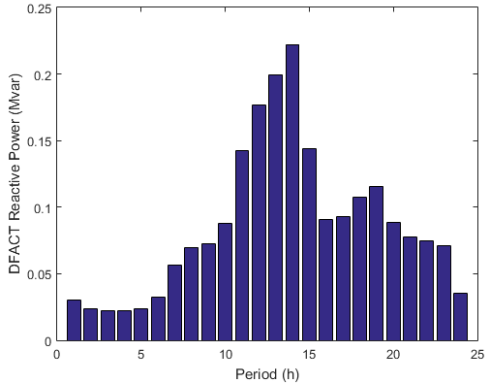

FIGURE 36. D-SVC behavior at scenario 7.

With the implementation of the reactive control in different devices, the voltage levels increase significantly, in a way that all buses present values inside of the adequate range during all day, as seen in Fig. 37.

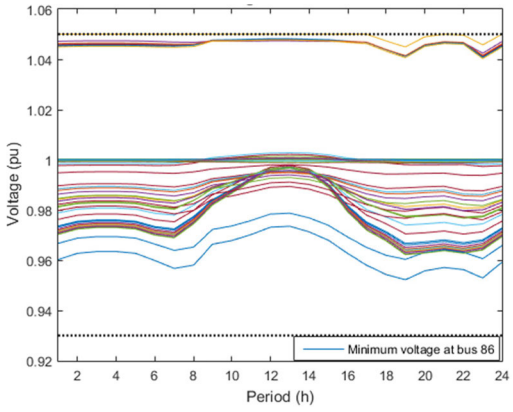

FIGURE 37. Voltage behavior for all 90 buses at scenario 7.

Concerning the microgrid operation in scenario 7, just small changes were required by the DSO, being the biggest one at the MG located at bus 64, in which is proposed a load reduction at 7h and 22h, being this demand relocated during the period from 2-5h and at 8h, as shown at Fig. 38.

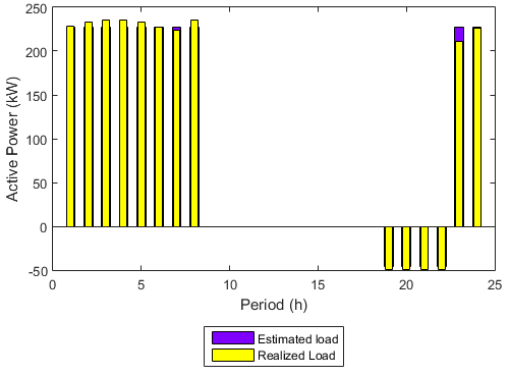

FIGURE 38. Estimated and realized load profiles for the microgrid placed at bus 64 at scenario 7.

Regarding the optimization convergence of the MPOPF for scenario 7, it happened in 29 iterations.

VI. REAL FEEDER SIMULATION RESULTS

As presented at section III.C, the objective function of the MPOPF has some weights defined to distribute the importance of the multiple goals that are being optimized.

Those values are defined by the execution of innumerous tests and combinations until the best simulation results is achieved. As aforementioned, the sum of all weights should be equals to one, so a normalization process can be performed.

For the real feeder simulations, the values of the weights for each simulation scenario are presented at Table 6.

TABLE 6. Normalized values of objective function weights.

Weights	Base Case	RF*+MG	RF+MG +PV	RF+MG +PV+BESS
wc	0.5	0.045	0.045	0.036
wp	0.5	0.045	0.045	0.036
wbat	-	-	-	0.163
wload	-	-	-	0.036
wgd	-	0.455	0.455	0.363
$w_{targetload}$	-	0.455	0.455	0.363

*RF: Real Feeder

A. REAL FEEDER – BASE CASE

For the real feeder, the base case corresponds to the current grid configuration, i.e. with the only load installed. The total daily energy consumption is, 27 MWh for summer months and 100 MWh for winter. Considering these load demand and the load behavior for the two scenarios considered, this feeder presents total power losses of 0.35% (94 kWh) and a total operational cost of 2,687.48 USD for summer, and 1,26% (1.26 MWh) of losses and 9,987.78 USD of cost for winter load profiles.

The active power balance in this scenario is presented in Fig. 39 (summer) and Fig. 40 (winter), being all the power load supplies by substation power injection.

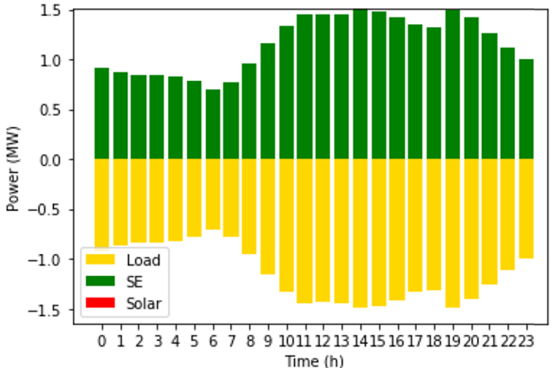

FIGURE 39. Active power balance for real distribution feeder on base case scenario for summer (SE is the substation bus).

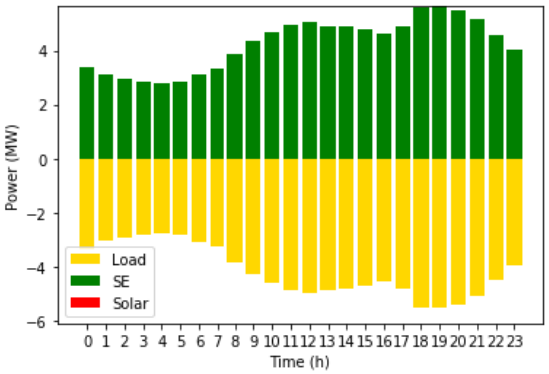

FIGURE 40. Active power balance for real distribution feeder on base case scenario for winter.

Voltage behavior for all buses is presented in Fig. 41 and 42, in which is seen the voltage levels at the substation bus as previously defined in Table 2. For all other circuit buses, there are no voltage violations, and the behavior changes following the corresponding load variation.

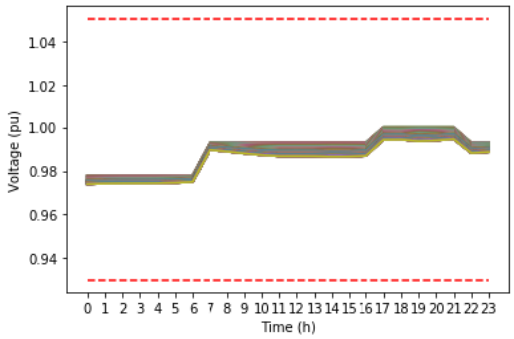

FIGURE 41. Voltage behavior for all buses in real feeder base case for summer load profile.

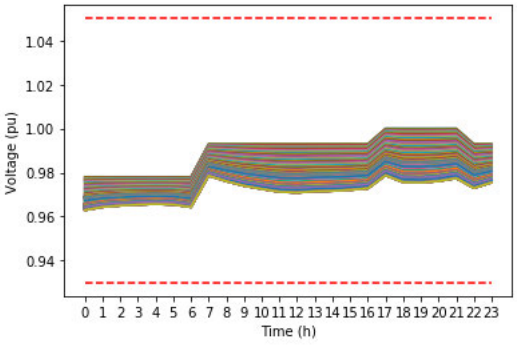

FIGURE 42. Voltage behavior for all buses in real feeder base case for winter load profile.

B. REAL FEEDER WITH THE CONNECTION OF THE PILOT MICROGRID

For the operation of the pilot microgrid, an internal optimization was developed and result in the load profiles shown in Fig. 9 and 10. This load profile was applied at the bus where the microgrid is connected.

From the results, the operational costs were lower than in the base case scenario. This happens since there is power injection from the microgrid during some periods and the power demand in this point of the circuit is also lower in comparison to the case when it was just a load. The values obtained with the MG operation are presented in Table 7.

TABLE 7. Results from the real feeder with microgrid connection for different load and microgrid profiles.

Real Feeder with MG	Power Losses	Operational Costs
Summer Profiles	0,33%	2,630.44 USD
Winter Profiles	1.27%	10,103.89 USD

Concerning the voltage behavior, it was similar to the one seen for the base case scenario (Fig. 40 and 41) since the levels of power injected and consumed by the microgrid are small compared to the feeder demand.

Regarding the behavior of the microgrid, there was no need to propose another operation point for it since the result of its internal planning allowed a feasible operation of the power grid.

Fig. 43 presented the active power balance with the small power injection from the microgrid (black).

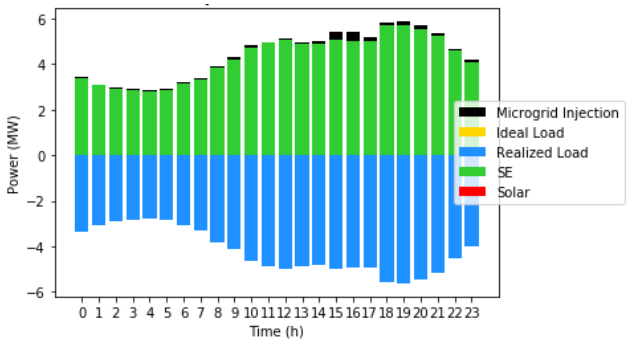

FIGURE 43. Active power balance for real distribution feeder with the connection of the microgrid for winter.

C. REAL FEEDER AS ACTIVE DISTRIBUTION NETWORK

Considering a future scenario in which the feeder starts to present the connection of more distributed energy resources in addition to the microgrid, the analysis was performed assuming a 30% penetration of distributed generation in this feeder. The allocation of this penetration was done proportionally in the load buses, considering that part of the equivalent loads modeled in each bus may present PV systems.

Table 8 shows the results when it was simulated the 30% of PV penetration during summer and winter scenarios of load and MG.

With the introduction of solar photovoltaic generation the power losses decrease, since part of the load is supplied by the existing generation nearby, reducing the amount of energy that needs to be delivered by the substation. In terms of voltage behavior, there is an increase in voltage values

TABLE 8. Results from real feeder with microgrid connection for 30% of pv penetration at summer and winter scenarios.

30% PV penetration scenarios	Power Losses	Operational Costs
Summer	0,26%	2,327.06 USD
Winter	1,02%	8,969.46 USD

during the solar generation period for almost all buses, as seen in Fig. 44 in comparison with Fig. 41.

At least, a BESS was connected in a point of the where 80% of the load is located downstream. For this analysis 30% of PV penetration was considered and the scenarios of summer and winter were evaluated.

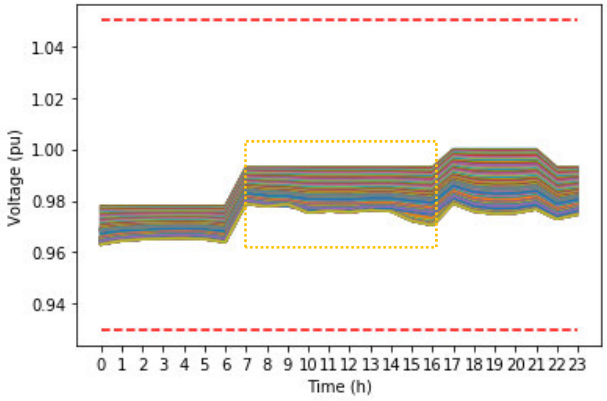

FIGURE 44. Voltage behavior for all buses in real feeder for winter load profile with microgrid and 30% of PV penetration. Highlight for the period with voltage increase.

From the results presented at Table 9, it is verified that power losses get reduced when compared to the scenario with only loads, since BESS can contribute to provide power closer to loads. In terms of operational costs, they are also lower than in previous scenarios due to the operation of BESS, that realizes the discharge during most costly period (regarding that white tariff is being considered), as show at Fig. 45.

Battery operational behavior both for summer and winter are similar, presenting the behavior illustrated at Fig. 45, in which the charging process occurs during the day (lower tariff and PV generation) and the discharge happens during the high tariff cost period.

TABLE 9. Results from the real feeder with microgrid connection, 30% of pv penetration, and bess.

Real Feeder + MG + 30% PV + BESS	Power Losses	Operational Costs	BESS Degradation Costs
Summer	1.01%	2,293.94 USD	445.25 USD
Winter	1.58%	8,886.76 USD	1,105.31 USD

Regarding voltage behavior, when BESS discharge happened, the voltage profile increased along all buses (Fig. 46) due to the injection of active and reactive power (BESS is operating with pf = 0,92). Active power injection close to

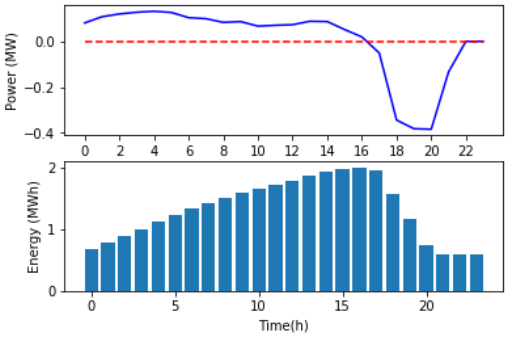

FIGURE 45. BESS power and energy behavior when connected to the real feeder with winter load profile and 30% of PV penetration.

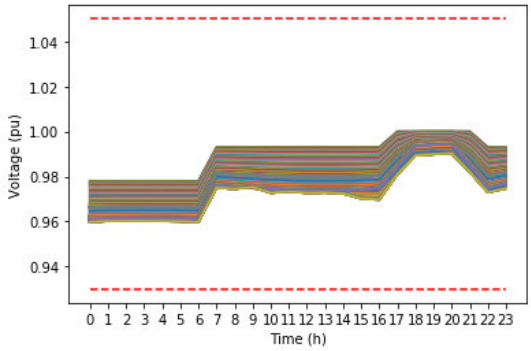

FIGURE 46. Voltage behavior for all buses in real feeder for winter load profile with microgrid, 30% of PV penetration and BESS.

load center and during the peak demand contribute to supply the load, with lower losses, contributing to increase voltage levels.

This is a robust distribution feeder, since it does not present any power quality problem, even with the connection of active elements as microgrid, distributed generation and BESS. This is an example of a distribution feeder that is currently ready for future grid transformations.

D. COMPUTATIONAL PERFORMANCE

The computational performance of the simulations with the real distribution feeder was also evaluated. It is important to highlight that all the problem formulation was implemented in Python language, not been used any solver or even toolbox.

Using the pre-processing step to organize the matrices (Fig. 11), the times of the optimization process for the different scenarios simulated are presented at Table 10. These

TABLE 10. Optimization times for different simulation scenarios with real distribution feeder with initialization based on previous simulations.

SCENARIO	SUMMER		WINTER	
	TIME (MIN)	NI**	TIME (MIN)	NI
BASE CASE	1.595	3	1.609	2
RF* + MG	2.390	5	2.459	5
RF+MG +PV	1.965	4	2.781	5
RF+MG+ PV+BESS	5.213	12	5.117	12

*RF: Real Feeder; ** NI: number of interations

time values were obtained in a computer with 16GB of RAM memory and Spyder IDE was used to run the Python script.

Initially the simulation is performed with a typical variables initialization, resulting in a higher number of interactions and higher performance time. Once the scenario had already been simulated, for the next time it uses the solution of the previous one to variables initialization, allowing to improve the optimization performance, since it starts close to the optimum point.

VII. CONCLUSION

Distribution grids are facing the biggest changes in their operation, mainly due to the insertion of new elements as distributed energy resources. In this way, it is necessary to model these new elements allowing the distribution system operator to plan the power grid operation inside of power quality levels.

The multiperiod optimum power flow proposed in the current work consists of a tool to optimize the entire grid operation, with the insertion of DERs considering different scenarios of its operation.

Additionally, the insertion of DERs and its active power provisioning through the main grid, the ancillary service of reactive power control was also considered in the MPOPF. In this way, a reactive dispatch from equipment that present inverters were done by the optimization methodology, resulting in improvements of voltage levels.

With the idea of an ADN scenario in mind, new equipment as D-FACTS were also considered connected to the main distribution grid. For this work, a D-SVC was placed in a branch with voltage problems, and its operation was also optimized, allowing to improve voltage levels, power losses, and the hosting capacity of DG into the distribution grid.

First, the 90 buses test feeder was evaluated in a different scenario, from a base case only with load, voltage regulator, and fixed capacitor banks to a scenario with PV, BESS, DSM, MGs, D-SVC, and VEs all connected simultaneously to the main grid.

At least a real distribution feeder, that currently present only loads, was evaluated with the insertion of distributed generation and a BESS, allowing the analysis of how this equipment can impact real distribution system operation. In this case, the proposed MPOPF also proved to be a robust simulation tool for real systems, even when the circuit grows in complexity.

REFERENCES

[1] M. Vadari, R. Melton, and K. Schneider, "Distribution operations: The evolution of distributed energy resources [guest editorial]," *IEEE Power Energy Mag.*, vol. 18, no. 1, pp. 14–16, Jan. 2020, doi: 10.1109/MPE.2019.2945342.

[2] Task Force C6.11. (2011). *Development and Operation of Active Distribution Networks*. [Online]. Available: https://e-cigre.org/publication/457-development-and-operation-of-active-distribution-networks

[3] Brazilian National System Operator–ONS. (2017). *Guidelines and Criteria for Electrical Studies–Submodule 23.3*. [Online]. Available: http://www.ons.org.br/%2FProcedimentosDeRede

[4] M. Ebeed, S. Kamel, and F. Jurado, "Optimal power flow using recent optimization techniques," in *Classical and Recent Aspects of Power System Optimization*. Amsterdam, The Netherlands: Elsevier, 2018, pp. 157–183.

[5] A. Gabash and P. Li, "On variable reverse power flow–Part I: Active-reactive optimal power flow with reactive power of wind stations," *Energies*, vol. 9, no. 3, p. 121, Feb. 2016. [Online]. Available: https://www.mdpi.com/1996-1073/9/3/121

[6] Y. Riffonneau, S. Bacha, F. Barruel, and S. Ploix, "Optimal power flow management for grid connected PV systems with batteries," *IEEE Trans. Sustain. Energy*, vol. 2, no. 3, pp. 309–320, Jul. 2011. [Online]. Available: http://ieeexplore.ieee.org/abstract/document/5713847/

[7] D. Gayme and U. Topcu, "Optimal power flow with large-scale storage integration," *IEEE Trans. Power Syst.*, vol. 28, no. 2, pp. 709–717, May 2013. [Online]. Available: https://ieeexplore.ieee.org/abstract/document/6313956/

[8] C. Wang, T. Liu, Z. Zhu, J. Cheng, C. Wei, Y. Wu, C. Lin, and F. Bai, "A probabilistic day-ahead scheduling with considering wind power curtailment," in *Proc. IEEE Conf. Energy Internet Energy Syst. Integr. (EI2)*, Nov. 2017, pp. 1–5. [Online]. Available: https://ieeexplore.ieee.org/abstract/document/8245338/

[9] N. Jayasekara, M. A. S. Masoum, and P. J. Wolfs, "Optimal operation of distributed energy storage systems to improve distribution network load and generation hosting capability," *IEEE Trans. Sustain. Energy*, vol. 7, no. 1, pp. 250–261, Jan. 2016. [Online]. Available: http://ieeexplore.ieee.org/abstract/document/7321810/

[10] L. Zhang and Y. Li, "Optimal energy management of wind-battery hybrid power system with two-scale dynamic programming," *IEEE Trans. Sustain. Energy*, vol. 4, no. 3, pp. 765–773, Jul. 2013. [Online]. Available: http://ieeexplore.ieee.org/abstract/document/6482285/

[11] E. Reihani, S. Sepasi, L. R. Roose, and M. Matsuura, "Energy management at the distribution grid using a battery energy storage system (BESS)," *Int. J. Electr. Power Energy Syst.*, vol. 77, pp. 337–344, May 2016. [Online]. Available: http://www.sciencedirect.com/science/article/pii/S014206151500455X

[12] M. Usman and F. Capitanescu, "A stochastic multi-period AC optimal power flow for provision of flexibility services in smart grids," in *Proc. IEEE Madrid PowerTech*, 2021, doi: 10.1109/PowerTech46648.2021.9495045.

[13] J. Yi, C. Pages, A. Allahham, D. Giaouris, and C. Patsios, "Modelling and simulation of a smartgrid architecture for a real distribution network in the UK," *J. Eng.*, vol. 2019, no. 8, pp. 5415–5418, Aug. 2019.

[14] M. A. Abdel-Moamen and N. P. Padhy, "Optimal power flow incorporating FACTS devices–bibliography and survey," in *Proc. IEEE PES Transmiss. Distrib. Conf. Expo.*, Sep. 2003, pp. 669–676, doi: 10.1109/TDC.2003.1335357.

[15] M. Basu, "Optimal power flow with FACTS devices using differential evolution," *Int. J. Electr. Power Energy Syst.*, vol. 30, no. 2, pp. 150–156, Feb. 2008, doi: 10.1016/j.ijepes.2007.06.011.

[16] S. Liu, Y. Hong, T. Ding, Z. Bie, and Y. Wu, "Optimal power flow with series static voltage restorer (SSVR) in distribution systems considering PV integration," in *Proc. IEEE PES Asia–Pacific Power Energy Eng. Conf. (APPEEC)*, Oct. 2016, pp. 104–109, doi: 10.1109/APPEEC.2016.7779479.

[17] P. M. B. de Freitas, R. K. Portelinha, and O. L. Tortelli, "D-SVC controller analysis in active distribution systems operation," in *Proc. IEEE PES Innov. Smart Grid Technol. Conf.-Latin Amer. (ISGT Latin America)*, Sep. 2019, pp. 1–6. [Online]. Available: https://ieeexplore.ieee.org/abstract/document/8895467/

[18] S. Granville, F. C. Mello, and A. C. G. Mello, "Application of interior point methods to power flow unsolvability," *IEEE Trans. Power Syst.*, vol. 11, no. 2, pp. 1096–1103, May 1996.

[19] M. R. Carvalho, "Estudo comparativo de fluxo de potência para sistemas de distribuição radial," M.S. thesis, Universidade de São Carlos, São Carlos, Brazil, 2006. [Online]. Available: https://www.teses.usp.br/teses/disponiveis/18/18133/tde-27072006-164213/publico/Dissertacao_Marcus_corrigida_vs_final.pdf

[20] R. R. Paiva, "Fluxo de potência ótimo em redes de distribuição de energia com a presença de geração distribuída: Um novo algoritmo para auxiliar a análise do perfil de tensão," M.S. thesis, Federal Univ. Santa Catarina, Florianópolis, Brazil, 2006.

[21] S. Borges, T. S. P. Fernandes, and K. C. Almeida, "Pré-despacho hidrotérmico de potência ativa e reativa via método dos pontos interiores e coordenadas retangulares," *Rev. Control Automação*, vol. 22, no. 5, pp. 479–494, 2011.

[22] ANEEL. (2021). *Geração Distribuída Aneel*. Accessed: May 5, 2021. [Online]. Available: http://www2.aneel.gov.br/scg/gd/GD_Fonte.asp

[23] *Technical Brochure 435-Ancillary Services: An Overview of International Practices*, Cigre, Paris, France, 2010.

[24] M. J. Afzal, A. Arshad, S. Ahmed, S. B. Tariq, and S. A. A. Kazmi, "A review of DGs and FACTS in power distribution network: Methodologies and objectives," in *Proc. Int. Conf. Comput., Math. Eng. Technol. (iCoMET)*, Mar. 2018, pp. 1–7. [Online]. Available: https://ieeexplore.ieee.org/abstract/document/8346405/

[25] T. M. Blasi, "Planning of active distribution systems operations with batteries and renewable energy sources," M.S. thesis, Federal Univ. Paraná, Curitiba, Brazil, 2020. [Online]. Available: https://acervodigital.ufpr.br/bitstream/handle/1884/67163/R%20-%20D%20-%20THAIS%20MARZALEK%20BLASI.pdf?sequence=1&isAllowed=y

[26] INPE. (2019). *Centro de Previsão de Tempo e Estudos Climáticos*. Accessed: Jun. 6, 2019. [Online]. Available: https://www.cptec.inpe.br/glossario.shtml

[27] E. E. C. Moraes, S. J. de Mesquita, R. P. S. Leao, M. B. M. Neto, K. Q. da Silva, R. M. C. Correa, H. A. dos Santos, L. Cajuaz, K. P. dos Santos, and F. R. Leite, "The application of D-STATCOM in smart distribution grid with wind power plants," in *Proc. 10th IEEE/IAS Int. Conf. Ind. Appl.*, Nov. 2012, pp. 1–6, doi: 10.1109/INDUSCON.2012.6453881.

[28] F. Relić, P. Marić, H. Glavać, and I. Petrović, "Influence of FACTS device implementation on performance of distribution network with integrated renewable energy sources," *Energies*, vol. 13, no. 20, p. 5516, Oct. 2020, doi: 10.3390/en13205516.

[29] A. R. Baran Junior, T. S. Piazza Fernandes, and R. A. Borba, "Voltage regulation planning for distribution networks using multi-scenario three-phase optimal power flow," *Energies*, vol. 13, no. 1, p. 159, Dec. 2019, doi: 10.3390/en13010159.

[30] T. S. P. Fernandes, "An optimal power dispatch model for multi-user systems," Ph.D. dissertation, Federal Univ. Santa Catarina, Florianópolis, Brazil, 2004.

[31] M. Sufyan, N. A. Rahim, M. M. Aman, C. K. Tan, and S. R. S. Raihan, "Sizing and applications of battery energy storage technologies in smart grid system: A review," *J. Renew. Sustain. Energy*, vol. 11, no. 1, Jan. 2019, Art. no. 014105, doi: 10.1063/1.5063866.

[32] H. Tazvinga, B. Zhu, and X. Xia, "Optimal power flow management for distributed energy resources with batteries," *Energy Convers. Manage.*, vol. 102, pp. 104–110, Sep. 2015.

[33] ANEEL. (2018). *Procedimentos de Distribuição de Energia Elétrica no Sistema Elétrico Nacional–PRODIST Módulo 8—Qualidade de Energia Elétrica*. [Online]. Available: http://www.aneel.gov.br/documents/656827/14866914/M?dulo_8-Revis?o_10/2f7cb862-e9d7-3295-729a-b619ac6baab9

[34] COPEL. (2019). *Tarifa Branca*. [Online]. Available: https://www.copel.com/hpcopel/root/nivel2.jsp?endereco=%2Fhpcopel%2Findustrial%2Fpagcopel2.nsf%2Fdocs%2FB0CA4C8DF4B62F98832581F00058CCF9

[35] A. A. Godoi, A. R. Aoki, and T. S. Fernandes, "Alocação ótima de bancos de capacitores em redes de distribuição de energia elétrica," in *Proc. 8th Conf. Bras. Sobre Qualidade de Energia Elétrica*, 2009, pp. 1–6.

[36] F. J. Lachovicz, "Planejamento de suporte de reativo para rede de distribuição com forte penetração de geração solar fotovoltaica," M.S. thesis, Federal Univ. Paraná, Curitiba, Brazil, 2018. [Online]. Available: https://acervodigital.ufpr.br/bitstream/handle/1884/57480/R%20-%20D%20-%20FELIPE%20JOSE%20LACHOVICZ.pdf?sequence=1&isAllowed=y

[37] M. E. Baran and F. Wu, "Optimal capacitor placement on radial distribution systems," *IEEE Trans. Power Del.*, vol. 4, no. 1, pp. 725–734, Jan. 1989.

[38] A. Gerossier, R. Girard, and G. Kariniotakis, "Modeling and forecasting electric vehicle consumption profiles," *Energies*, vol. 12, no. 7, p. 1341, Apr. 2019, doi: 10.3390/en12071341.

[39] K. C. Divya and J. Østergaard, "Battery energy storage technology for power systems—An overview," *Electr. Power Syst. Res.*, vol. 79, pp. 511–520, Apr. 2009.

[40] *NTC 905100–Acesso de Geração Distribuída ao Sistema da Copel (com Comercialização de Energia)*, COPEL, Curitiba, Brazil, 2017.

THAÍS M. BLASI was born in Brazil, in 1995. She received the B.S. and M.Sc. degrees in electrical engineering from the Federal University of Paraná, Brazil, in 2017 and 2020, respectively, where she is currently pursuing the Ph.D. degree with the Department of Electrical Engineering. In 2018, she developed part of her master's research at Technische Hochschule Ingolstadt, Germany, in conjunction with the Institut für neue Energie-Systeme (InES). Since 2016, she has been actuating in research and development projects in electric power systems. Her research interests include optimization planning of electric power systems, active distribution networks, microgrids, and electric mobility.

THELMA S. P. FERNANDES was born in Brazil, in 1964. She received the M.S. and Ph.D. degrees in electrical engineering from the Federal University of Santa Catarina, Florianópolis, Brazil, in 1989 and 2004, respectively. Since 1990, she has been a Professor and a Researcher with the Federal University of Parana. Her research interest includes optimization applied to the operation planning of electrical power systems.

ALEXANDRE R. AOKI (Senior Member, IEEE) was born in Brazil, in 1974. He received the B.S., M.Sc., and Ph.D. degrees in electrical engineering from Itajuba Federal University (UNIFEI), Itajuba, Brazil, in 1996, 1999, and 2003, respectively. He was a Senior Researcher and a Manager with the Institute of Technology for Development (Lactec Institutes), from 2003 to 2017. He was a Professor with the Development of Technology, Lactec Institutes, from 2004 to 2017, and a Coordinator, from 2010 to 2014. Since 2008, he has been a Professor with the Federal University of Paraná, Curitiba, Paraná, Brazil. His research interests include planning and operation studies for distribution systems and smart grid, including renewable energy sources and storage systems. He serves for a number of committees related to distributed generation and smart grids, including IEEE and CIGRÉ.

FABRÍCIO H. TABARRO was born in Brazil. He received the B.S. degree in informatics from the State University of Ponta Grossa. He is currently a Manager of Quality Technology Division, Copel Distribution's Service Channel.